



1 Research Article

2 Stratigraphic modeling of the Western Taiwan foreland
3 basin: sediment flux from a growing mountain range
4 and tectonic implications5 Stefan Nagel ^a, Didier Granjeon ^b, Sean Willett ^a, Andrew Tien-Shun Lin ^c,
6 Sébastien Castelltort ^{a,d,*}7 ^a Department of Earth Sciences, ETH Zürich, Sonneggstrasse 5, 8092 Zürich, Switzerland8 ^b IFP Energies Nouvelles, Rueil-Malmaison, Paris, France9 ^c Department of Earth Sciences, National Central University, 300 Jungha Road, Chungli, Taoyuan 101, Taiwan10 ^d Department of Earth Sciences, University of Geneva, Rue des Maraichers 13, 1205 Geneva, Switzerland

11

12 *Keywords*

13 Taiwan

14 Foreland basin

15 Tectonic sedimentology

16 Arc-continent collision

17 Stratigraphic modeling

18 Erosion

19 Sedimentation

20

21 **ABSTRACT**

22 Sediment flux signals in foreland basins preserve a record of tectonics, sea level and climate through
23 erosion and sedimentation. However, longitudinal sediment transport often occurs in foreland basin,
24 thus removing part of the orogenic material flux from foreland basins. Here we use mass balance
25 calculation and stratigraphic simulations of sediment fluxes for the Taiwan orogen to provide a
26 quantified order of magnitude estimate of how much orogenic material may bypass a foreland basin.
27 Our results indicate a significant, potentially more than 50%, mismatch between sediment volume
28 currently preserved in the basin and the amount of material eroded from the orogen since the onset of
29 collision in Taiwan. This supports previous paleogeographic work suggesting that longitudinal
30 sediment transport in the paleo-Taiwan Strait served as a bypass conduit important for the
31 establishment of a steady state orogen. We identify candidate submarine topography in the South
32 China Sea that may preserve Taiwan's missing erosional mass.

33

34 **1. Introduction**

35 Sediment fluxes within foreland basins exert a primary control on basin architecture involving
36 interactions between tectonics, sea level and climate through erosion and sedimentation (e.g.,
37 Castelltort et al., 2015). The orogenic history of many ancient basins has been reconstructed with help

* Corresponding author. Tel: +41 223796616

E-mail address: sebastien.castelltort@unige.ch (S. Castelltort)

38 of the sedimentary record, such as the Alps (Garzanti et al., 2004; Lihou and Allen, 1996), the
39 Pyrenees (Puigdefàbregas et al., 1992; Vergés and Burbank, 1996), or the Himalayas (Garzanti et al.,
40 2005; White et al., 2002), but it is still not well known how much of the orogenic history is eventually
41 preserved and how tectonics, facies and sediment supply to basins are linked (Castelltort et al., 2015).

42 The western foreland basin in Taiwan is an excellent place to study interactions between tectonics and
43 sediment fluxes because it is very young and still very active. In this basin, the southwestward ongoing
44 oblique collision between the volcanic arc with the continental shelf makes it possible to record the
45 full evolution of the basin deformation (Suppe, 1981) and provides an opportunity to connect tectonics
46 and depositional processes at different stages of the basin's evolution.

47 The Taiwan orogen is emblematic of the distinct classical evolutionary stages that characterize many
48 ancient foreland basin systems such as the Molasse basin of the Alps (Allen et al., 1991), the Bradanic
49 Trough in the Appennines (Tropeano et al., 2002) or the Solomon Sea in Papua New Guinea (Silver et
50 al., 1991). The western foredeep in Taiwan evolved from an early underfilled stage with relatively
51 deep-water sedimentation to a late balanced-filled stage, where shallow marine environments persist
52 until today (Covey, 1984), despite the enormous amount of sediment supplied to the ocean by the
53 rising Taiwan mountains (Milliman and Kao, 2005; Milliman and Syvitski, 1992).

54 It is well known that the Taiwanese collision formed a time-transgressive southwestward oriented
55 migration of facies belts (Nagel et al., 2012c) and sediment depocenters (Simoes and Avouac, 2006),
56 similar to other oblique collisions (e.g. Papua New Guinea, Abbott et al., 1994; Silver et al., 1991), but
57 the geometry of the initial collision is still ambiguous and several models have been proposed.
58 Whereas some models favor an arc - continent collision (Huang et al., 2006; Suppe, 1984, 1988; Teng,
59 1990), others suggested a two stage collision of an exotic block with the Eurasian continental margin
60 and a second collision of the Luzon volcanic arc with the passive margin (Lu and Hsü, 1992), or an arc
61 - arc collision between the Luzon volcanic arc with a paleo - Ryukyu arc system extending to the west
62 of Taiwan (Seno and Kawanishi, 2009; Sibuet and Hsu, 1997; Sibuet et al., 1995), or even that the
63 collision may have happened synchronously along the entire margin length (Castelltort et al., 2011,
64 Lee et al., 2015).

65 It is also known that the orogenic system in Taiwan reached an approximately constant mountain
66 width of 90 km, which has been interpreted as being an expression of topographic steady state (Stolar
67 et al., 2007; Suppe, 1981). Additional observations also show that the Western foredeep eventually
68 reached a steady state size where accommodation space stayed constant despite the large sediment
69 fluxes from Taiwan mountains (Covey, 1984; Covey, 1986). Therefore Covey (1986) suggested that
70 sediment bypass out of the basin must have been an important factor that balanced accommodation
71 space and sediment supply, maintaining the basin shallow marine, and preventing it from becoming
72 overfilled or even fully terrestrial.

73 In this study, a 3D stratigraphic model is used to test different tectonic scenarios for the orogen
74 evolution and how basin architecture corresponds. The model is calibrated with seismic lines from the
75 Taiwan Strait. We show how different tectonic settings control the stratigraphic evolution of a
76 foreland basin. This also involves a quantitative estimation of the sediment-volume budget for the
77 basin and provides information on the importance of longitudinal sediment transport out of the basin.

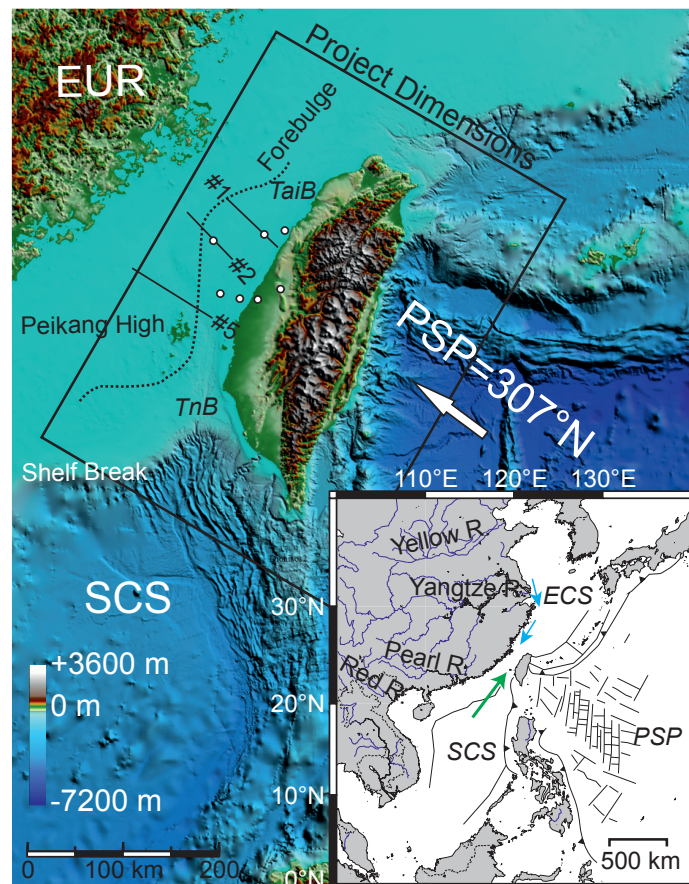
78

79 **2. General setting and background**

80 *2.1. Geology and Tectonics*

81 The Taiwan mountains, rising almost 4 km above sea level, formed by the collision between the
82 Philippine Sea plate and the Eurasian continental shelf. Arc volcanism associated with the subduction of
83 the Philippine sea plate ceased between 6 Ma and 3 Ma, when the arc resisted subduction and collided

84 with the Asian passive margin to form an initial accretionary wedge (Huang et al., 2006; Yang et al.,
 85 1995). The arc-continent collision is estimated to have initiated in late Pliocene (Nagel et al., 2012c).
 86 This is based on observing a continuous sandstone provenance shift and increasing illite crystallinity,
 87 interpreted to represent the progressive unroofing and recycling of the metamorphic orogenic belt
 88 (Dorsey et al., 1988; Nagel et al., 2012c). The oblique collision between the N-S trending Luzon
 89 volcanic arc and the NE-SW trending passive margin resulted in a southwest propagating collision
 90 (e.g., Nagel et al., 2012c; Simoes and Avouac, 2006; Suppe, 1981; Teng, 1990) and the modern
 91 collision point is presently located in the offshore SW Taiwan (Lin et al., 2008; Yu and Huang, 2009).
 92 The easternmost part of the South China Sea is currently being subducted below the Philippine sea
 93 plate along the Manila Trench whereas the Philippine sea plate itself is being subducted northwards
 94 below the Eurasian plate (Kao et al., 2000) together with high active seismicity and a convergence rate
 95 of 70 - 80 km/Ma between the Philippine sea plate and the Eurasian continent (Seno et al., 1993; Wu
 96 et al., 2009; Wu et al., 2007; Yu et al., 1997). The current plate convergence is mainly accommodated
 97 within the Longitudinal Valley Fault on the east coast and at the deformation front in the Western
 98 Foothills consistent with the main active faults (Yu et al., 1997).
 99 The continental margin experienced extensive rifting and continental breakup phases due to the
 100 opening of the South China Sea in late Paleogene, which resulted in major subsidence and numerous
 101 sub-basins separated by topographic highs (Lee and Lawver, 1995; Lin et al., 2003). The orogen is
 102 divided into different tectonic units (Fig. 1) consisting of the accreted volcanic arc (e.g. Coastal
 103 Range) separated by the suture zone (e.g. Longitudinal Valley Fault), the main orogenic belt (e.g.
 104 Central Range), the deformed and uplifted foreland basin strata which constitutes a classical fold-and-
 105 thrust belt (e.g. Western Foothills), and the undeformed onshore (e.g. Coastal Plain) and offshore
 106 foreland basin sediments (Ho, 1988).
 107



141 influenced environments, which became progressively dominated by fluvial processes upsection. This
 142 is the main foreland basin stage driven by large sediment fluxes out of the Taiwan orogen and
 143 southward migration of facies belts. During the late Pleistocene, increased erosion lead to the
 144 deposition of large alluvial sediments which most likely are an ancient example of braided rivers
 145 draining the orogen today (Covey, 1984).

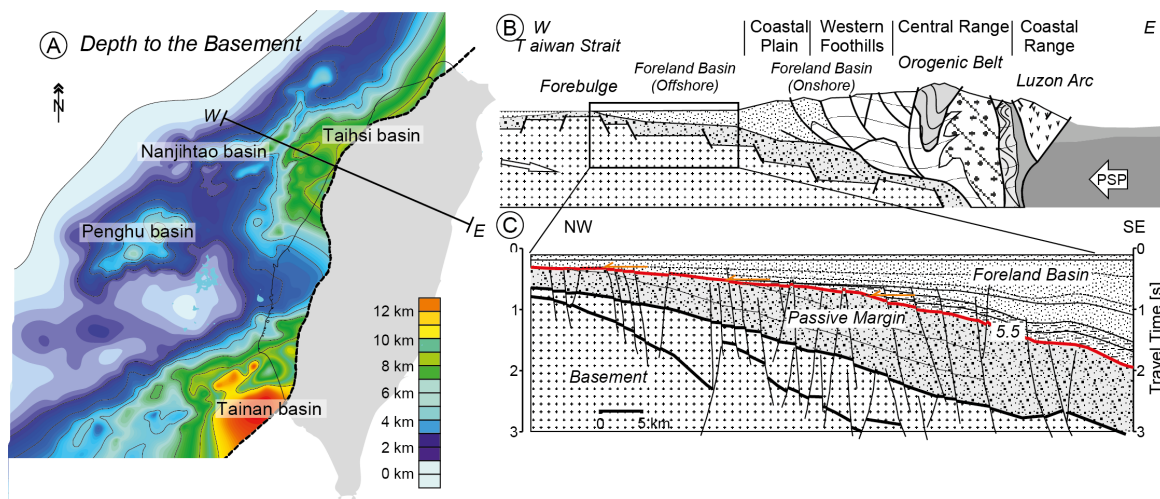
146

147 2.2. The foreland basin unconformity

148 The age of collision onset and its kinematics are still controversial. Most authors consider a collision
 149 age between 6.5 Ma and 3 Ma assuming a single arc-continent collision (e.g., Chang and Chi, 1983;
 150 Dorsey and Lundberg, 1988; Huang et al., 2006; Lin et al., 2003; Pelletier and Stephan, 1986; Suppe,
 151 1981; Teng, 1990) or a two stage collision (e.g. arc-arc and arc-passive margin) between 12 Ma and
 152 3Ma respectively (Lu and Hsü, 1992; Seno and Kawanishi, 2009; Sibuet and Hsu, 1997; Sibuet et al.,
 153 1995).

154 The flexural response due to the loading of the Eurasian shelf by the forming orogen and its
 155 sedimentary response has been studied in detail (Castelltort et al., 2011; Chen et al., 2001a; Chiang et
 156 al., 2004; Simoes and Avouac, 2006; Tensi et al., 2006). Tensi et al. (2006) suggested that the passive
 157 margin lithosphere already experienced flexure since 12.5 Ma and interpreted the observed flexure as
 158 not being related to the initial arc-continent collision, which is consistent with plate kinematic
 159 reconstructions (Hall, 1996; Nagel et al., 2012a; Sibuet and Hsu, 2004). The basal foreland
 160 unconformity is observed in the Northern basins (e.g. Taishi basin, Fig. 3) with an age estimated
 161 between 8.6 and 5.6 Ma (based on biostratigraphic data), consistent with a flexural migration of the
 162 load from east to west (Lin and Watts, 2002; Lin et al., 2003). This unconformity separates the passive
 163 margin sequence and the foreland basin sequence, which onlaps onto it. The depositional hiatus
 164 increases in duration from the current frontal thrust towards the forebulge in the middle of the Taiwan
 165 Strait (Lin et al., 2003; Yu and Chou, 2001).

166



167

168

169 **Figure 3:** A) Map of depth to the Cenozoic basement in Taiwan's foreland, highlighting four individual basins separated by
 170 basement highs. The Nanjihtao basin is partially covered by a distal foreland basin sequence. The Taishi and Tainan basin are
 171 separated by the Peikang High. Figure modified from Lin and Watts (2003). B) Schematic cross section of the Taiwan orogen
 172 in the north, where the interpreted forebulge topography is most pronounced. C) Detailed seismic line drawing modified from
 173 Yu and Chou (2001). The foreland basin sequence onlaps onto passive margin deposits, with increasing depositional hiatus
 174 towards the forebulge, where late Pleistocene-Quaternary sediments directly overlie Miocene strata.

175

176 2.3. Modern sediment fluxes in Taiwan

177 The East Asian monsoonal climate was most probably established since 8.5 Ma (e.g. late Miocene)
178 with an intensification observed since 5 to 3 Ma (Liu et al., 2003; Wan et al., 2006; Zheng et al.,
179 2004). Today the island experiences 4 to 6 typhoons with maximum mean annual rainfall of 2000-
180 3000 mm yr⁻¹ (Kao and Milliman, 2008). The total annual amount of sediment delivered to the ocean
181 by Taiwanese rivers has been estimated to be up to 500 Mtyr⁻¹ with a strong asymmetry across the
182 mountain range (Dadson et al., 2003; Liu et al., 2008). Estimates of erosion rates range between 2.2 to
183 8.3 mmyr⁻¹ (Dadson et al., 2003; Fuller et al., 2003) and up to 30 mmyr⁻¹ (Resentini et al., 2017) in
184 agreement with quantitative estimates from thermochronometric constraints of 3 to 10 mmyr⁻¹ (Lee et
185 al., 2006; Willett et al., 2003).

186 Much of the suspended sediment is delivered at hyperpycnal concentrations into the Taiwan Strait
187 (Dadson et al., 2005; Milliman and Kao, 2005; Milliman et al., 2007) where it is redistributed by
188 seasonal and tidal currents (Jan et al., 2002). The northeast directed South China Sea current (Fig. 1),
189 for example, transports warm tropical water into the Strait with a peak intensity during the summer
190 month (June to August), in contrast to the southwest directed China Coastal current (Fig. 1), which can
191 deliver small portions of Yangtze-derived mud into the northern Taiwan Strait (Hu et al., 2010; Xu et
192 al., 2009) during winter month (September to May). The morphology of the sea floor as well as the
193 seasonal variation in temperature and salinity exert an important control on the distribution of grain
194 size in the modern sediments and may help to understand the occurrence of different facies in the
195 ancient sedimentary record (Liao et al., 2008; Yang and Chun, 2001).

196 Marine observations indicate that fine mud particles are relatively quickly transported northward out
197 of the Taiwan Strait (Horng and Huh, 2011; Horng et al., 2012; Huh et al., 2011; Liu et al., 2010). For
198 example, marine investigations in the Choshui river delta made before and after a typhoon hit the
199 island, showed that fine-size particles are redistributed and transported northward within a month
200 (Milliman et al., 2007).

201 Average sedimentation rates vary greatly from 2 mm yr⁻¹ in the Western foreland basin to 3-4 mmyr⁻¹
202 in the Coastal Range (Chen et al., 2001a; Lin et al., 2003; Lundberg and Dorsey, 1990), with a rapid
203 increase observed since the onset of deformation in the Western Foothills (Chang et al., 1983; Lock,
204 2007; Mouthereau and Lacombe, 2006; Mouthereau et al., 2001). These values are in accordance with
205 erosion rates estimates of between 2 and 10 mm yr⁻¹ from modern river sediment loads and
206 interpretation of thermochronological data (Dadson et al., 2003; Fuller et al., 2003; Fuller et al., 2006;
207 Liu et al., 2001; Liu et al., 2000; Siame et al., 2011; Simoes et al., 2007; Simoes and Avouac, 2006;
208 Willett et al., 2003)(Table 1).

Author/Year	Uplift (U)/Exhumation Rate (E) [mm/a]	Erosion Rate/Incision Rate (I) [mm/a]
Peng et al. (1977)	U: 5±0.7 (<9 ka) Holocene coral reefs ¹	
Liu (1982)	U: 4.2-6.8 (3-0.5 Ma) 8.9±1.9 (<0.6 Ma)	
Jahn et al. (1986)	U: 3-4 (<3 Ma) Rb-Sr isotopes (TC)	
Lundberg and Dorsey (1990)	U: 5.9-7.5 (<1.3-0.9 Ma) CoR	6-7 (<1 Ma)
Wang and Burnett (1990)	U: 1.2-6.1 10 ka (Holocene) ²	
Chen et al. (1991)	U: 5-14 (<5000 a) (CoR, uplifted corals)	
Liew et al. (1993)	U: 2.5-8 (Holocene) elevated shoreline deposits (CoR)	
Lo and Onstott (1995)	E: 1.7-1.6 (K-Ar reset ages)	
Liu (1995)	U: 36-42 (<10a, GPS, CR)	
Liu et al. (2000, 2001)		2.5-4.6 (<4 Ma) 2.3-6 (TC) ZFT/AFT
Hsieh and Knuepfer (2002)	U: <10 (Holocene river terrace)	I: <20 (river incision)
Dadson et al. (2003)	E: 3-6 (ECR) 1.5-2.5 (SW Taiwan)	5.2 (<30a) SSC ³ 6 (CR), up to 60 ⁴ I:1.5-9 (Holocene)
Fuller et al. (2003)		2.2-8.3 (8-27a, SSC)
Willett et al. (2003)		7-8 4-6 (AFT/ZFT)
Yamaguchi and Ota (2004)	U: 5-15 (<13 ka) Holocene marine terraces (CoR)	
Song et al. (2004)	U: 10.9, 5.4 Holocene marine terraces (CoR)	
Simoès and Avouac (2006); Simoès et al. (2007b,a) ⁵		4.2 (BR)-6.3 (TC) 2-3 (<1.5 Ma)
Fuller et al. (2006)	E: 3-5 (acceleration since 2-1 Ma)	2.3-3.3 (AFT/ZFT ⁶) max. 6 - 8
Lee et al. (2006)	U: <1 (6-1 Ma) 4-10 (<1 Ma)	
Siame et al. (2011)		2 ±1 (<100 ka), 5-7 (<50 a) ⁷
Kuo-En (2011)	U: 0.2-18.5 (2000-2008, GPS) (BR)	
Siame et al. (2012)		I: 0.8±0.1 - 10.1±1.3 (<300 ka) (Choshui river terraces)

¹Hengchun Peninsula, Tainan area, Coastal Range²Hengchun Peninsula, Coastal Range, Lanyu and Lutao³SSC=calculation based on modern suspended sediment concentrations⁴active thrust faults, Western Foothills, Southwest Taiwan⁵thermokinematic modeling⁶AFT=Apatite fission track, ZFT=Zircon fission track⁷Be10, Lanyang catchment

209

210

Table 1: Summary of observed and predicted kinematic data for the Taiwan orogen.

211

3. Data sets and methods

212

3.1. 3D stratigraphic model "Dionisos"

213

214

To evaluate the complex relationships between the stratigraphic record, tectonics (e.g. subsidence, with respect to the initial collisional geometry) and climate (e.g. erosion rates), the stratigraphic model Dionisos was used (Granjeon, 1997). Dionisos is a process-based modelling tool using a diffusion and advection law that links sediment flux to local slope (e.g. potential available energy to move sediment) and water flow (e.g. transport efficiency of the lithologies defined) by a diffusion coefficient. Erosion

215

216

217

218

219 and sedimentation at each point of the basin are defined by combining the transport equation and the
220 law of mass conservation:

$$Q_{sed} = -K \cdot Q_{water} \cdot \overrightarrow{grad} h$$

221 The second basic assumption of the model is the law of mass conservation

$$\frac{\partial h}{\partial t} = -div Q_{sed}$$

222 where:

223 Q_{sed} = sediment transport [m^2/s]

224 Q_{water} = relative water flow [-]

225 K = diffusion coefficient [m^2/yr]

226 h = ground elevation [m]

227 $\delta h/\delta x$ = elevation gradient (i.e., slope)

228 Boundary supplies (i.e. sediment volume and sand, mud fraction), water discharge of rivers at source
229 locations and rainfall are defined for each sedimentary sequence. It is important to note that all the
230 water introduced by the rivers and rainfall is conserved and flows towards the lowest part of the basin
231 (Granjeon and Joseph, 1999). The potential sediment availability is simulated by a maximum erosion
232 rate, which depends on climate (e.g. rainfall), subsidence rate and uplift rate (e.g. topographic
233 elevation).

234 The study area was set as a 500 km x 320 km rectangle in the Taiwan Strait where abundant data is
235 available (Fig. 1). It is confined to the flexural forebulge in the West and the Coastal Range in the
236 East, and includes the Taishi basin in the North and the Tainan Basin in the South (Fig. 1). The main
237 input data required by Dionisos consist of tectonic subsidence for different time intervals, sediment
238 supply and eustatic sea level fluctuations (e.g. climatic influence), compaction, flexure and sediment
239 transport parameters. Sediment influx corresponds either to a predefined boundary condition into or
240 out of the study area or to basement erosion.

241 The input data was acquired from published boreholes and seismic lines offshore in the Taiwan Strait
242 and onshore (Lin and Watts, 2002; Lin et al., 2003; Yu and Chou, 2001), together with constructed
243 depth maps (Fig. 4) for five key stratigraphic horizons defined in an earlier study (Nagel et al., 2012c)
244 provide a solid first approximation database.

245

246 3.2. Foreland basin subsidence

247 The most important basin-scale controls on accommodation include flexural tectonics related to
248 tectonic loads and sea level changes. The West Taiwan basin formed by flexural bending of the Asian
249 passive margin in front of the westward migrating thrust loads of the growing accretionary wedge (Lin
250 et al., 2003). In order to better constrain the subsidence of the sedimentary basin, backstripping
251 techniques (using Airy isostasy) were applied to 28 boreholes and 9 stratigraphic sections (Nagel et
252 al., 2012c; Watts and Ryan, 1976).

253 Backstripping is used to stepwise decompact and unload a borehole or stratigraphic section from the
254 influence of water and sediments and, therefore, to isolate the contribution of the tectonic forces
255 responsible for subsidence. The tectonically driven subsidence at any location in the basin is given in
256 Allen and Allen (2009):

$$TS = Y \cdot \left(\frac{\rho_m - \rho_s}{\rho_m - \rho_w} \right) - \Delta sl \cdot \left(\frac{\rho_w}{\rho_m - \rho_w} \right) + (W_d - \Delta sl)$$

257 where:

258 W_d = the average water depth at which the sedimentary units were deposited

259 Y = decompacted sediment thickness

260 $\rho_m/\rho_w/\rho_s$ = densities of the mantle, the water and mean sediment density

261 Δsl = the difference in sea-level height h between the present and the time at which the sediments
262 were deposited:

$$\Delta sl = \left(\frac{\rho_m - \rho_w}{\rho_m} \right) \cdot (h_2 - h_1)$$

263 The water depth at the time of deposition for the backstripped strata was estimated by applying the
264 depositional model constructed by Nagel et al.(2012c). Note that since the sediments in the western
265 foreland basin were deposited on a shallow marine continental shelf, the influence of the water column
266 (10s of metres) on the backstripped strata is small relative to the considered thicknesses (100s of
267 metres). Sediment was assumed to be composed of two main grain size classes, sand and mud, which
268 correspond to the modern siliciclastic river supply and is consistent with detailed lithologic analysis
269 (Huh et al., 2011; Nagel et al., 2012c). When the basin gets progressively filled with sediments,
270 mechanical compaction introduces loss of water during sediment burial and affects the depth-porosity
271 curves for different lithologies. The trend between porosity and depth is usually approximated by:

$$\phi = \phi_0 \cdot e^{-cy}$$

272 This produces an asymptotically low porosity with increasing depth, where ϕ_0 describes the surface
273 porosity and c the coefficient of compaction (Table 2). The flexure of the basement was computed
274 with an elastic thickness of 15 km, a Young's modulus of 100 GPa and a Poisson's ratio of 0.25. These
275 values are in agreement with recently published values for the Taiwan foreland basin (Lin and Watts,
276 2002).

277

Lithology	Surface porosity [ϕ_0]	Compaction coefficient [km^{-1}]	Density [kg/m^{-3}]
Shales	0.63	0.51	2720
Sandstones	0.49	0.27	2650
Mudstones	0.56	0.39	2680
Water			1030
Mantle			3330

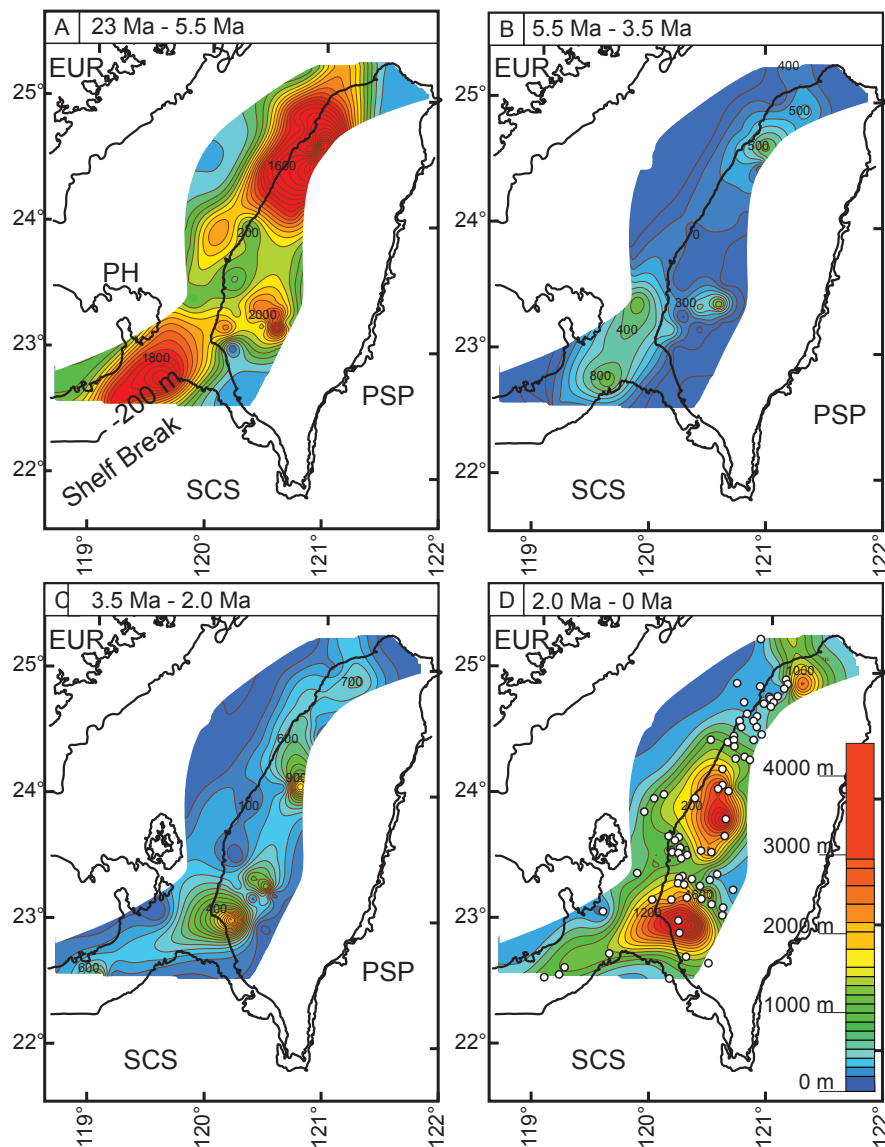
278

279 **Table 2:** Values used in the backstripping for the different lithologies observed in the Western Taiwan foreland basin and
280 compaction coefficient (after (Allen and Allen, 2009; Lin et al., 2003; Tensi et al., 2006).

281

282 The backstripping results provide a detailed record of the Asian passive margin subsidence and uplift
283 history at five key biostratigraphic horizons (Fig. 4). Lin and Watts (2003) showed that the subsidence
284 history of the Asian passive margin is strongly influenced by its syn- and post-rift history due to the
285 extension in the South China Sea (e.g. post-breakup extension from 30 to 21 Ma, thermal subsidence
286 from 21 to 12.5 Ma and a second post-breakup extension from 12.5 to 6.5 Ma). The increased
287 subsidence since the early Pliocene is ascribed to the growth of the Taiwan orogen as it propagates
288 westward, introducing deformation and increasing sedimentation rates in the basin (Chang and Chi,
289 1983; Mouthereau et al., 2001). In addition, Tensi et al. (2006) demonstrated that the load associated
290 with the initial foreland basin has migrated rapidly westward 1 Ma ago and was stabilized at the same
291 time as the basin was buried under large quantities of sediments (e.g. alluvial and fluvial fans of the
292 Toukoshan fm.).

293



294

295 **Figure 4:** Maps of decompacted sediment thickness in between the five key biostratigraphic (nannofossils) horizons of Nagel
 296 et al (2013).

297

298 The reconstructed subsidence pattern is consistent with sediment isopach maps shown in Figure 4. Lin
 299 and Watts (2002) showed that the topography is insufficiently high to produce the observed
 300 subsidence pattern in an isostatic flexural model driven by surface loads. Following Simpson (2014), it
 301 can be proposed that this observation is an illustration of a possible decoupling between subsidence
 302 and surface loads, especially prominent in deeply eroded mountain ranges. In his model, Simpson
 303 explains that what may have been previously attributed to “buried loads” (as in Taiwan, e.g. Lin and
 304 Watts, 2002) could be related to the accumulation though time of vertical deformation due to repeated
 305 large seismic events and the dragging of the foreland margin by reverse slip on the main orogenic
 306 front.

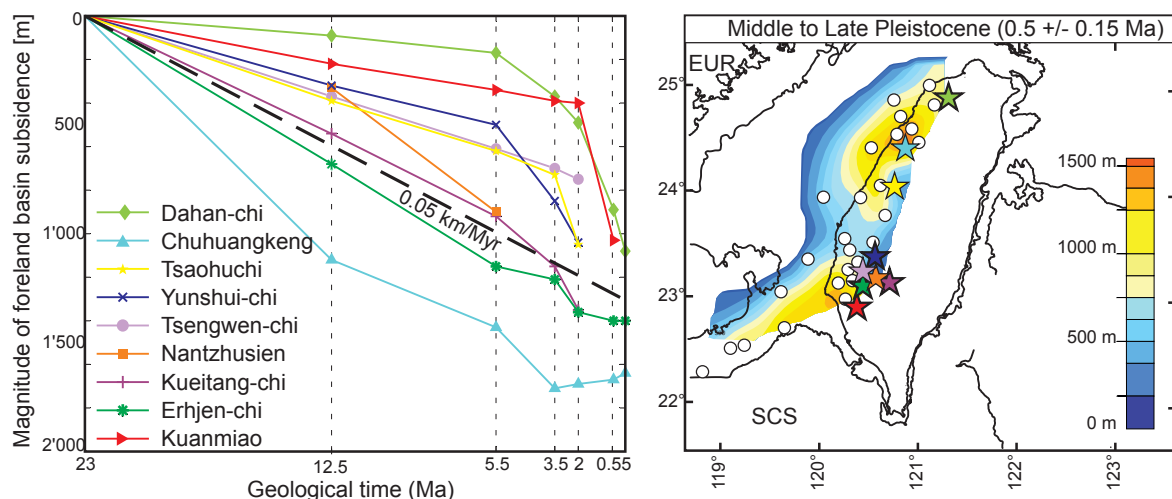
307

308 3.3. Sediment fluxes and basin boundaries

309 The volume of sediment deposited in the basin was calculated from data of published boreholes drilled
 310 by the CPC (Chinese Petroleum Corporation) in the western foreland basin (Fig. 4) (e.g., Lin et al.,
 311 2003; Shaw, 1996). For each sequence the sediment thickness is extrapolated between the present day

312 forebulge and the Western Foothills by a triangulation algorithm to obtain four maps between the early
 313 Miocene and late Pleistocene. The chronostratigraphy of the Western Foothills has been extensively
 314 studied with Neogene calcareous nannofossils (Chang and Chi, 1983; Chou, 1973; Huang, 1977;
 315 Huang and Huang, 1984) and builds the basis for the five key biostratigraphic horizons that are best
 316 documented (Nagel et al., 2013). Two main depositional basins are recognized throughout the
 317 Neogene: the Tainan basin in the South and the Taishi basin in the North (Fig. 3). During most of the
 318 Miocene, sediment accumulation rates were low, but started to increase in late Miocene to early
 319 Pliocene (Chang and Chi, 1983). The early Pliocene shallow-water Kueichulin formation is generally
 320 associated with the latest pre-orogenic deposition on the passive margin and the relative sea level rise
 321 recorded in the transition from Kueichulin to Chinshui formations marks the onset of load induced
 322 subsidence by the growing accretionary wedge (Fig. 2). During the late Pliocene, the mud-dominated
 323 Chinshui Shale was deposited into an underfilled, but relatively shallow marine foreland basin (Covey,
 324 1984), which was then filled by the nearby orogenic wedge with fluvial and alluvial sediments during
 325 Toukoshan fm. It is important to note that in the modern Taiwan Strait, mud-sized grains are quickly
 326 transported northwards out of the Taiwan Strait (Milliman et al., 2007, Liu et al., 2008, Kao et al.,
 327 2008a, Huh et al., 2011) and that the sediments eroded from the orogen possibly contained a larger
 328 amount of mud than currently found in deposits, and that has been fractionated away by marine
 329 processes.

330



331 **Figure 5:** A) Tectonic subsidence histories from stratigraphic sections in the fold-and-thrust belt of Taiwan (marked with a
 332 star, ordered from north to south). Dahan-chi (Pan, 2011), Chuhuangkeng (Huang, 1976), Yunshuichi/Tsaohuchi (Yeh and
 333 Chang, 1991; Yeh and Yang, 1994), Tsengwen-chi (Chen et al., 2001a), Nantzhusien (Ting et al., 1991; Yu et al., 2008),
 334 Kueitangchi (Huang, 1977), Erhjen-chi (Horn and Shea, 1994), Kuanmiao (Chiu, 1975). B) Tectonic subsidence map for the
 335 late Pleistocene (NN19/20) with 28 boreholes and 9 stratigraphic sections. Stars indicate stratigraphic sections with color
 336 coding corresponding with left panel in which sections legend is ordered from North (top) to South (bottom).
 337
 338

339 The sediment volume accumulated within each time sequence is shown in Table 3. A total of 82-
 340 125'000 km³ of sediment accumulated since 5.5 Ma in the foreland basin of Taiwan. If we assume that
 341 the collision started between 5.5 Ma and 3.5 Ma, and that before 5.5 Ma the sediment thickness
 342 corresponded only to the influx of material from Asia mainland, we interpret the increasing sediment
 343 influx from the Taiwan orogenic wedge to be in the range of 6'500 to 28'000 km³/Ma (Table 3). This
 344 sediment flux estimate is probably overestimated since the basin also must have received material
 345 from its western border, i.e. Asia mainland. However, this contribution was swamped by the dramatic
 346 increase in sedimentation rates that accompanied Taiwan orogeny (Chang and Chi, 1983). In addition,
 347 some of the sediment transported into the foredeep consists of recycled foreland basin deposits.
 348 Therefore the calculated sedimentation rates over the area of the modern foreland basin are lower

349 when compared with sedimentation rates from the Western Foothills, especially during the last phase
 350 of orogenesis from 2 Ma to 0 Ma (Chang and Chi, 1983).

Age [Ma]	Sediment Volume [km ³]	Sediment Flux [km ³ /Ma]	Sediment Flux From Asia [km ³ /Ma]	Sediment Flux From Taiwan [km ³ /Ma]
0.0 - 2.0	47'214 - 64'884	23'607 - 32'442	..	17'864 - 28'203
2.0 - 3.5	20'443 - 35'980	13'628 - 23'987	..	7'885 - 19'748
<i>Total</i>	<i>67'657 - 100'864</i>			
3.5 - 5.5	15'917 - 26'502	7'959 - 13'251	..	6'594 - 9'012
5.5 - 23.5	76'298 - 103'383	4'239 - 5'743	4'239 - 5'743	0
<i>Total</i>	<i>159'872 - 230'749</i>			

351

Sediment Volumes SE Asia [km ³]		2 - 0 Ma	2 - 5 Ma	5 - 11 Ma	11 - 17 Ma	17 - 24 Ma	24 - 5 Ma	[km ³ /Ma]
Pearl River & S. Taiwan	Total	81000	93000	240000	85000	130000	455000	23947
	<i>uncertainty</i>	<i>40000</i>	<i>38000</i>	<i>100000</i>	<i>31000</i>	<i>49000</i>		
	min	61000	74000	190000	69500	105500	365000	19211
	max	101000	112000	290000	100500	154500	545000	28684
E. China Sea & N. Taiwan	Total	190000	200000	45000	39000	88000	172000	9053
	<i>uncertainty</i>	<i>81000</i>	<i>75000</i>	<i>16000</i>	<i>12000</i>	<i>31000</i>		
	min	149500	162500	37000	33000	72500	142500	7500
	max	230500	237500	53000	45000	103500	201500	10605
Okinawa Trough	Total	130000	99000	16000	5200	4900	26100	1374
	<i>uncertainty</i>	<i>64000</i>	<i>40000</i>	<i>6000</i>	<i>2000</i>	<i>2100</i>		
	min	98000	79000	13000	4200	3850	21050	1108
	max	162000	119000	19000	6200	5950	31150	1639
Total	Total	271000	293000	285000	124000	218000	653100	34374
	Min	210500	236500	227000	102500	178000	528550	27818
	Max	331500	349500	343000	145500	258000	777650	40929

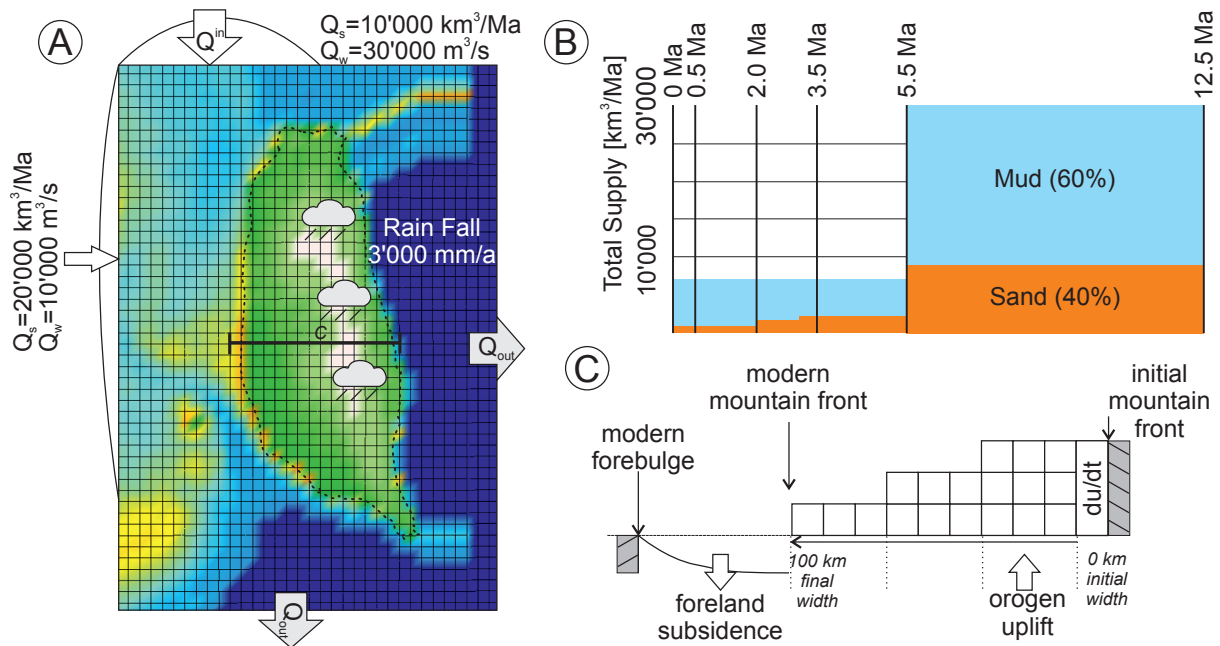
352 **Table 3:** Sediment volume accumulated during the Neogene on the Asian passive margin calculated for the area between the
 353 modern forebulge and the Western Foothills (ca. 35'000 km²). The age sub-division corresponds to biostratigraphic key
 354 horizons from nannofossil zonation (Nagel et al., 2013). The first two digits are considered significant.

355

356 **Table 4:** Sediment volume accumulated in the Cenozoic sedimentary basins of Southeast Asia (modified from, Métivier et
 357 al., 1999).

358

359 Sediment fluxes from the growing Taiwan orogen are delineated by comparing the amount of
 360 sediment that has been preserved in the Taiwan foreland basin with the amount of sediment
 361 accumulated in the Cenozoic sedimentary basins north and south of Taiwan (Table 4). The obtained
 362 boundary supply fluxes are minimum, because some unknown amount might have bypassed or not
 363 even reached the Taiwan Strait.



364
 365 **Figure 6:** Initial sediment supply history applied in the model. A) The two source areas correspond to Asia mainland (West)
 366 and the East China Sea (North). Rainfall follows the modern mean annual rainfall rate. The fluvial water discharge was
 367 estimated by modern river discharges in Southeast Asia (Table 5). B) The initial total sediment supply from the boundaries
 368 through time is based on the sediment preserved in the foreland basin and the sediment accumulation rates in Southeast Asia
 369 (Métivier et al., 1999). The grain size distribution follows modern suspended sediment concentrations and sea surface
 370 measurements in the Taiwan Strait (Huh et al., 2011; Kao and Milliman, 2008; Xu et al., 2009), as well as observations in the
 371 ancient sedimentary record (Nagel et al., 2013). See text for discussion. C) Sketch of orogen growth as implemented in
 372 Dionisos: the area of uplift rate is progressively enlarged to simulate mountain range widening, from 0 at the onset to 100 km
 373 width at the end.

374

375 Finally, the initial sediment supply history applied in the model is shown in Figure 6. Two source
 376 areas are defined along the western and northern model area (Fig. 1). It is important to note that these
 377 sources refer to general provenances located along the model boundaries and are not meant to
 378 represent individual rivers. Today, only the smaller tributaries of the Minjiang and Jiulong rivers drain
 379 directly into the Taiwan Strait, collectively discharging only 1/10 of the Taiwanese rivers (Table 5).
 380 The water discharge per source area was assumed to be similar to the modern water discharge of rivers
 381 in Southeast Asia (Table 5).

	catchment area [km^2]	mean channel gradient [m/km]	average water discharge [m^3/s]	dis- sediment load [km^3/a]	shelf gradient [m/km]
WORLD*					
Mississippi	2900000	0.5	17704	0.1481	8.0
Amazon	5700000	0.8	150000	0.4444	0.7
Ebro	85000	1.3	500	0.0074	3
Nile	4000000	1.6	2700	0.0889	4
Bengal	1750000	1.7	29700	0.3630	1.1
Indus	1400000	2.5	2644	0.1667	1.5
Sepik River	77700	0.05	3700	0.0288	6.50
Fly River	76000	-	6000	0.0315	0.76
Waiapu River	1734	-	1346	0.0181	5.00
SOUTHEAST ASIA**					
Yangtze	1940000	0.04	28507	0.1778	0.17
Red	124400	2	1200	0.0370	0.39
Pearl	440000	-	10654	0.0167	0.52
Yellow	750000	8.2	1160	0.4000	0.15
Minjiang	61000		6000	0.0028	
Jiulong	14700		1000	0.0009	
TAIWAN***					
Touchien	566	0.35	25	0.0078	2.3
Houlung	536	0.44	22	0.0181	1.8
Taan	758	0.34	36	0.0007	1.8
Tachia	1235	0.26	78	0.0011	1.4
Wu	2026	0.22	116	0.0019	0.8
Choshui	3155	0.18	120	0.0004	1.4
Peikang	645	0.06	27	0.0037	4.1
Pachang	475	0.24	23	0.0222	4.3
Tsengwen	1177	0.18	34	0.0007	4.3
Erjen	350	0.07	19	0.0007	5.0
Kaoping	3256	0.23	248	0.0059	5.0
Peinan	1603	0.44	97	0.0078	30.0
Hsiukuluan	1790	0.29	125	0.0130	50.0
Hualien	1507	0.4	100	0.0333	35.0
Hoping	556	0.37	37	0.0081	80.0
Lanyang	979	0.48	75	0.0111	13.0

*from Somme et al. 2009 and references therein, **Chen et al. 2001, Wang et al. 2005, Wang et al. 2007, Wang et al. 2008, Liu et al. 2007, Zhang et al. 2008, Olariu et al. 2009, Milliman and Syvitski 1992, Yu et al. 2006, Kineke et al. 2000, Huh et al. 2011, Kuehl et al. 2004, Kuehl et al. 2000, Yu et al. 1991, Wolanski et al. 1995, Kniskern et al. 2010, Hicks et al. 2000, ***Liu et al. 2008, Kao and Milliman 2008, Yu and Chiang 1997

382
383 **Table 5:** Main parameters of rivers from Taiwan, Southeast Asia and larger rivers worldwide for comparison. Data World
384 from Somme et al.(2009) and references therein. Data for Southeast Asia from Chen et al (2001b), Hicks et al (2000), Huh et
385 al (2011), Kineke et al (2000), Kniskern et al (2010), Kuehl et al (2004), Liu et al (2007), Milliman and Syvitski (1992),
386 Olariu and Steel (2009), Wang et al (2007), Wang et al (2005), Wolanski et al (1995), Yu et al (1991), Yu and Huang (2006)
387 and Zhang et al (2008), Data for Taiwan from Kao et al (2008), Kao and Milliman (2008), Liu et al (2008) and Yu et al
388 (1997).

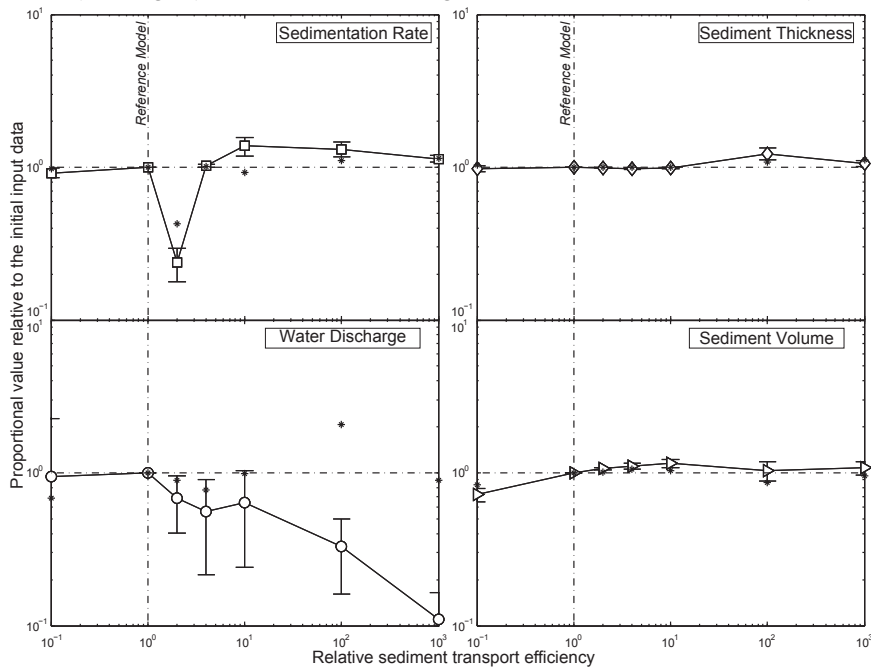
389
390 Since sediment transport in Dionisos is modeled by diffusion, a short review of published values for
391 the diffusivity coefficient K in different depositional environments is provided here for comparison
392 (Table 6). Although these cited modeling studies did not necessarily use diffusion in exactly the same
393 manner(for instance depending on whether water discharge is taken into consideration or not), an
394 average value for each depositional environment was used based on the values compiled in Table 6.

	Continental	Marine
Csato et al. (2007)	2000-4000	0.4-10
Clark et al. (2009)	1000-2000	0.01-1
Burgess et al. (2006)	125-500	2.5-10.0
Schlager and Adams (2001)	100	0.15
Flemings and Jordan (1989)	1-25.0	0.1-5
Jordan and Flemings (1991)	4-200	0.1-1
Sinclair et al. (1991)		0.5
Kaufman et al. (1991)		10.0-75
Rivenaes (1992)		0.05-10.0
Paola et al. (1992)	10.0-70.0	
Kenyon and Turcotte (1985)	24.0-560	
Naden et al. (1999)	191.0-3557	
Marr et al. (2000)	10-100	
Begin (1988)	4300	
Humphrey and Heller (1995)	0.25	

395
396 **Table 6** Ranges of diffusion coefficients used in modeling studies for individual depositional environments. The values were
397 converted to [km^2/ka].

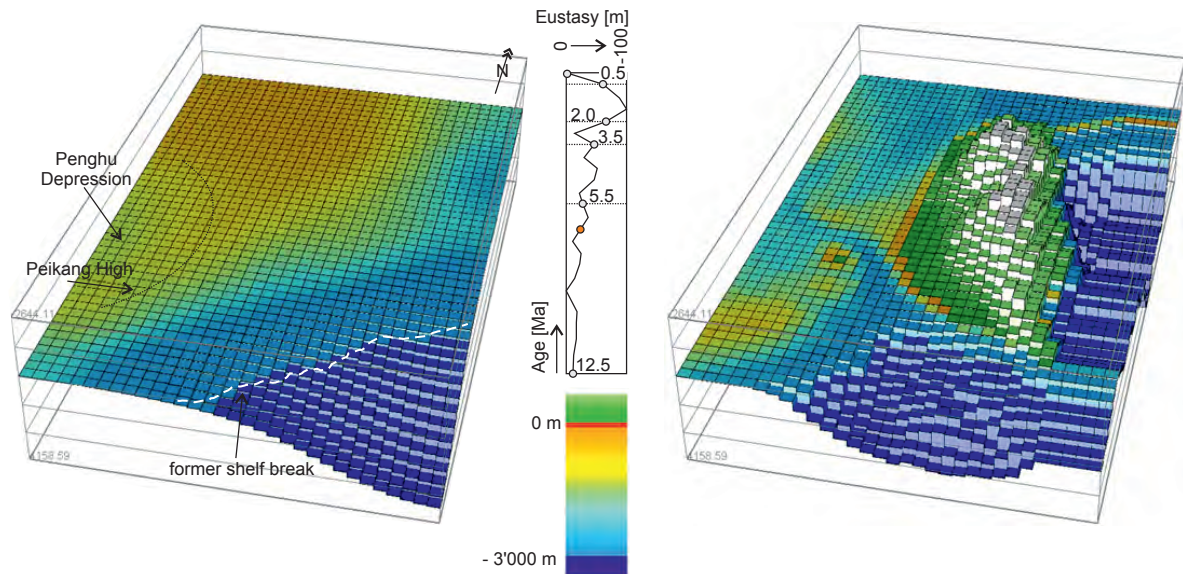
398

399 Figure 7 shows the sensitivity of different parameters (water discharge, sediment thickness, sediment
 400 volume, sedimentation rate) for 7 model runs with increasing sediment transport efficiencies (between
 401 $0.1 \times K_{\text{initial}}$ and $1000 \times K_{\text{initial}}$). All the models were run with the standard model set-up described above.
 402 The parameters were measured at three different points within the basin at seismic line L1-1, L1-2,
 403 L5-1 (see Fig. 1) as well as the average value from 3.5 Ma to 0 Ma (marked with asterisk).



404 **Figure 7:** Sensitivity test for different diffusion coefficients. Proportional values of the four measured parameters in relation
 405 to the initial model input data within the foreland basin, plotted against the relative efficiency of sediment transport. The
 406 results are from seven separate model runs with the same initial reference model parameters, but different diffusion
 407 coefficients.
 408

409
 410 The model starts at 12.5 Ma, which corresponds to the NN5-6 nannofossil boundary. This key
 411 biostratigraphic horizons have already been used in an earlier study to reconstruct the paleogeography
 412 during the arc-continent collision (Nagel et al., 2013). The study shows that the sedimentation in the
 413 foreland basin during the Miocene to Pleistocene took place in a mixed storm- and tide-dominated
 414 shallow marine depositional environment. The paleobathymetry did not change significantly from 12.5
 415 Ma to 3.5 Ma (Fig. 8), when the basin started to subside due to the approaching orogenic wedge in the
 416 east and the mud-dominated Chinshui Shale was deposited (Fig. 2). It is important to note that
 417 progradation and shallowing-upward cycles associated with the approaching orogenic wedge took
 418 place earlier in the northern parts of the basin and progressed southward as the basin was filling up
 419 (Nagel et al., 2012c).



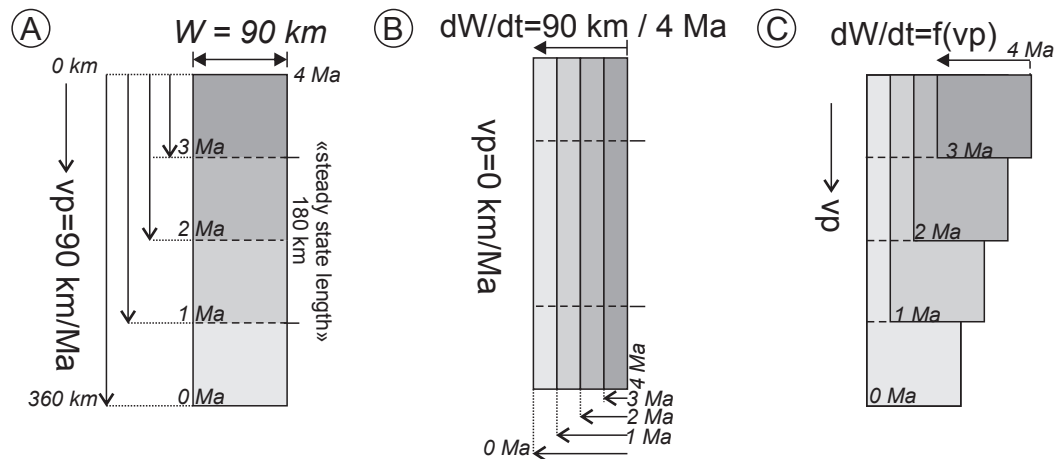
420

421 **Figure 8:** Initial bathymetry map at 12.5 Ma (left), and modern bathymetry (right). The 12.5 Ma map was constructed based
 422 on detailed facies analysis in the Western Foothills (Nagel et al., 2013). Sea level variation after Miller et al. (2011) for
 423 indication.

424

425 3.4. Experimental setup

426 To explore the orogen growth history and basin architecture, three different absolute tectonic scenarios
 427 were tested (Fig. 9). Each model considers the same initial boundary supply data (Fig. 6). In these
 428 experiments, orogenic uplift begins at ~ 4 Ma, which is in agreement with recent provenance studies
 429 (Nagel et al., 2013). The first orogenic growth model (Figure 9A) considers southward propagation of
 430 the orogen at a rate of 90 km/Ma until the present day length of 360 km is reached, and assumes a
 431 fixed steady state width of 90 km (Suppe, 1981). Using the time-space principle initially constructed
 432 by Suppe (1981), steady state size was reached after *ca* 1.3 Ma following the onset of orogeny. In a
 433 second model (Figure 9B) it is assumed that the orogen collided with a large promontory
 434 simultaneously along the length of the modern orogen, with no (or just minor) southward propagation.
 435 This scenario is based on sedimentological studies and paleogeographic reconstruction of Castellort et
 436 al (2011) and tectonic-thermochronometric data of Lee et al (2015). The third model intermediate
 437 between both previous ones, (Figure 9C) considers a linear growth in length of the orogen with time,
 438 along with lateral displacement of the orogen area as it overthrusts the Eurasian margin. In all three
 439 models, a continuous and constant uplift rate of 5 km/Ma was assumed. This rate covers the range of
 440 uplift rates published in Taiwan (Table 1).

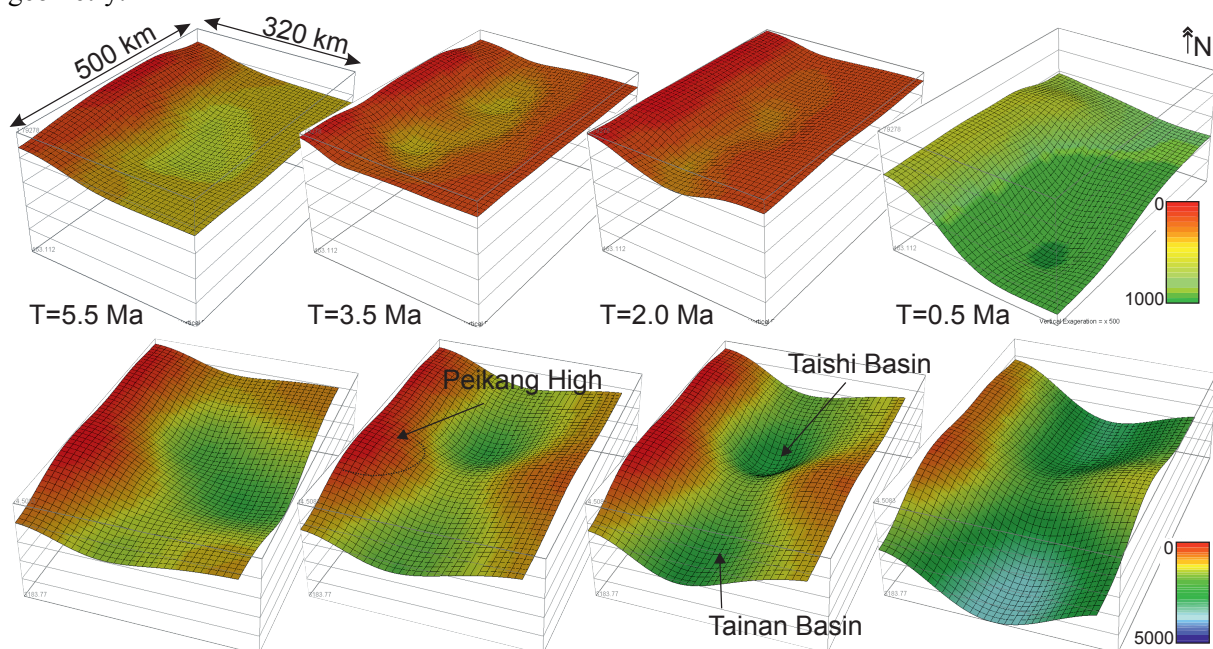


441
 442 **Figure 9:** Three orogen growth models tested in this study. A) Pure lengthening: southward propagation (90 km/Ma) of a
 443 steady state orogen with a fixed width of 90 km. B) Pure widening: lateral propagation, with a fixed length of 360 km. C)
 444 Lengthening and overthrusting: southwestward propagation of a steady state orogen.
 445

446 4. Simulation results and discussion

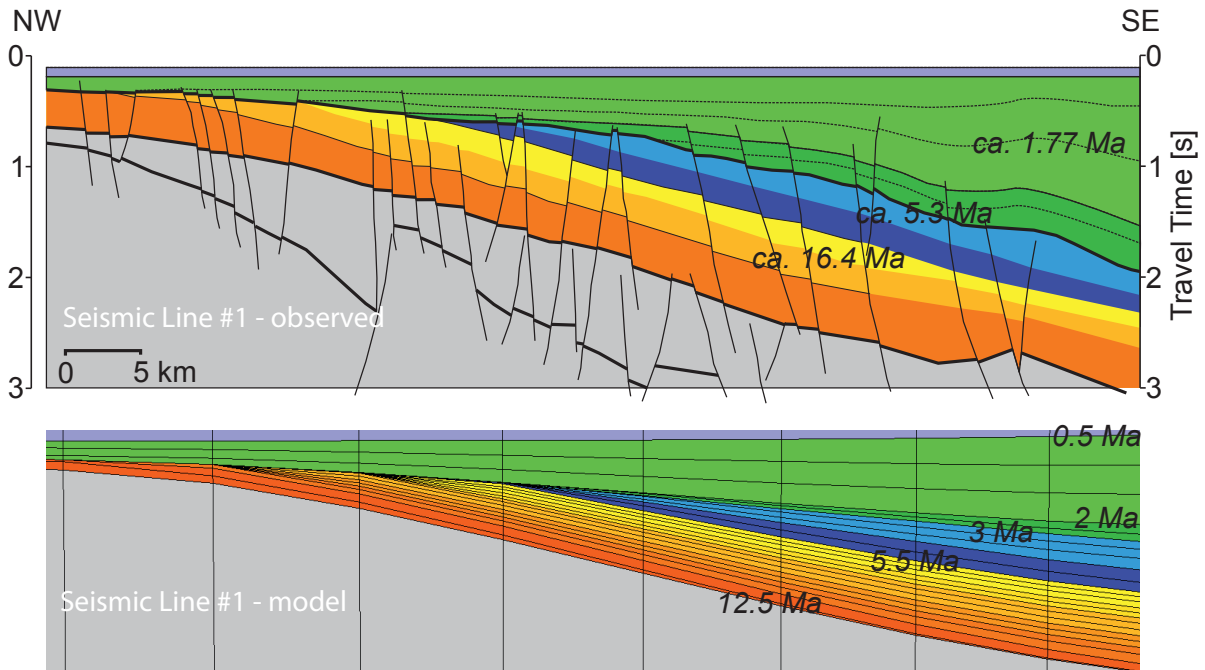
447 4.1. Foreland basin geometry

448 THE standard model setup needed to test the different tectonic scenarios (Fig. 9) is achieved by
 449 imposing subsidence maps for the different time intervals considered. The subsidence maps were
 450 constructed by first synthesizing the facies observed in the field into paleogeographic maps. These
 451 maps then provide an estimation of paleobathymetries for the entire basin (Nagel et al., 2013). Finally,
 452 the paleobathymetric estimates along with ages and sediment thicknesses are used to backstrip vertical
 453 sections in the basin, producing the subsidence maps (Fig. 10). An initial test of this approach is to try
 454 to recover the first order geometry observed on seismic lines in the Taiwan Strait (Fig. 3). A key
 455 horizon to compare is the transition from passive margin sedimentation to foreland basin
 456 sedimentation with its so-called "flexural forebulge unconformity". As shown in Figure 11, the
 457 imposed timing and subsidence results in sediment fluxes that correlate well with the observed
 458 geometry.



459

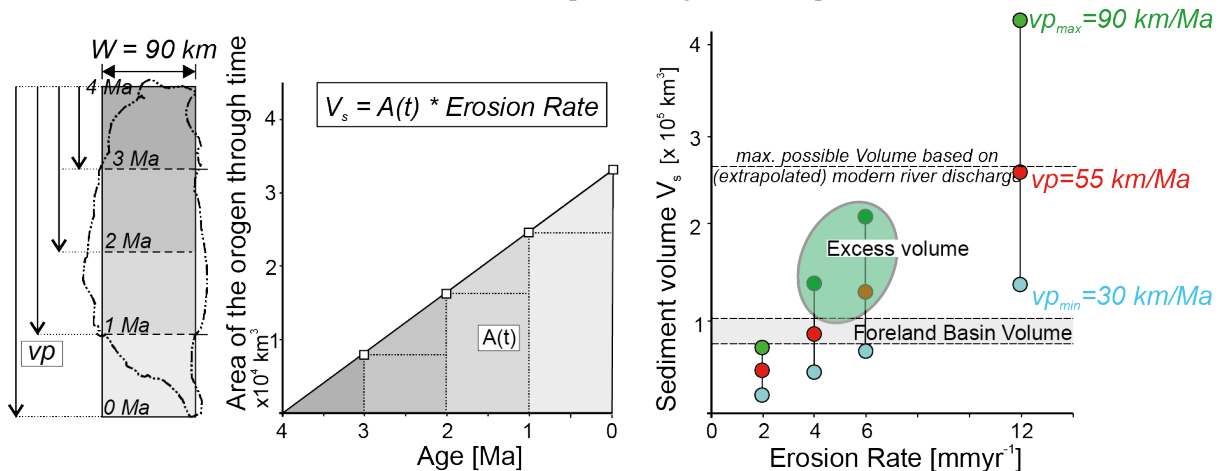
460 **Figure 10:** Smoothed subsidence maps for each simulated interval with tectonic subsidence used in the program (upper row)
 461 and total subsidence (including isostatic effects of sediment and water loading, lower row). The sediment depocenters in the
 462 north (e.g. Taishi basin) and the south (e.g. Tainan basin) are separated by the Peikang High.
 463



464 **Figure 11:** The input subsidence forces a dramatic change of sedimentation pattern at the transition from passive margin
 465 sedimentation to foreland sedimentation. This mimics the "flexural forebulge unconformity" documented by Yu and Chou
 466 (2001). This unconformity represents the boundary between the pre-collisional Nanchuang Fm. and the syn-collisional
 467 Kueichulin Fm. and was estimated approximately at 6.5 Ma (Lin et al., 2003).
 468
 469

470 *4.1. Mass flux calculations*

471 Theoretical models of mountain building propose that an orogen can reach a topographic steady state
 472 when the rates of rock uplift and erosion are balanced (Willett and Brandon, 2002). These models
 473 predict that, once steady state is reached, the sediment influx into the basin exceeds the available
 474 accommodation space, since no additional tectonic load is acting on the subsidence anymore, and
 475 therefore the basin becomes overfilled with time (Covey, 1986; Naylor and Sinclair, 2008). Despite
 476 observations suggesting that Taiwan has been in steady state since the Late Pliocene (Suppe, 1981,
 477 1984), or even increased in exhumation rate in the Pleistocene (Hsu et al., 2016), the Western Foreland
 478 basin is still not overfilled. This can be explained either by a large original accommodation space or a
 479 continuous removal of sediment from the basin preventing it to fill-up.



481 **Figure 12:** A) Orogen growth model with a steady state orogen width of 90 km and a southward propagation rate of $V_p=30$
 482 to 90 km/Ma. B) The theoretical volume eroded from the mountain was calculated by integrating the orogen area through
 483 time multiplied by the erosion rate. C) The modern river discharge was extrapolated over 3.5 Ma and taken as an upper limit
 484 for the maximum possible sediment influx into the basin system (Table 5). The theoretical sediment volume eroded from the
 485 mountains was corrected for the fluvial discharge flowing to the east, which is currently 45% (Dadson et al., 2003).

486

487 To explore sediment dynamics within the foreland basin, mass balance calculations were done for a
 488 southward propagating orogen model. The total amount of material transported into the basin
 489 (according to tectonic scenario of Fig. 12) is compared with the amount of sediment preserved. The
 490 theoretical total amount of material, which has been eroded from the orogen since 4 Ma, is estimated
 491 by multiplying the integrated area (Fig. 12) with the erosion rate (Table 1). Currently 55% of the
 492 annual fluvial sediment discharge is flowing to the west and 45% is drained to the east (Dadson et al.,
 493 2003; Liu et al., 2008). Hence the total sediment volume produced by the orogen was corrected for the
 494 fluvial discharge flowing to the east.

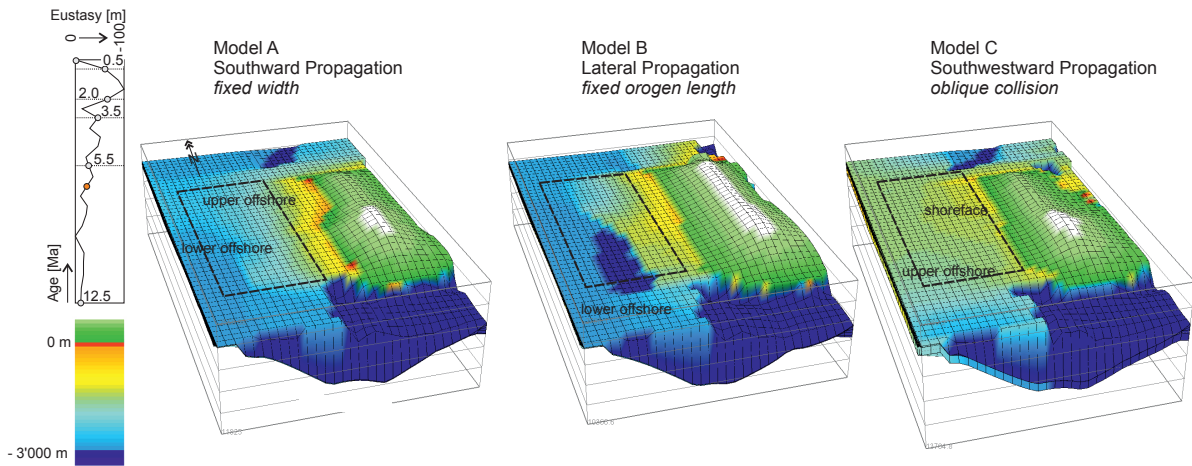
495 Figure 12 shows the potential sediment flux into the foredeep coming from the Taiwan mountains as
 496 estimated by the model. Computed fluxes vary from 25'000 km³ (for a southward propagation rate of
 497 30 km/Ma and an average erosion rate of 2 mm/yr) and up to 425'000 km³ (for a southward
 498 propagation rate of 90 km/Ma and an average erosion rate of 12 mm/yr), although this may be
 499 overestimated since it does not take into account the recycling of foredeep sediments. The current river
 500 sediment flux during typhoon season (Liu et al., 2008) was taken as an upper boundary for the
 501 maximum possible sediment influx, when extrapolated over 4 Ma (i.e., 285'000 km³).

502 Comparing both, the amount of sediment preserved in the basin (Fig. 4) with the possible amount of
 503 sediment carried into the basin (Fig. 12), with a southward propagation rate of 90 km/Ma, and
 504 assuming an average upper and lower erosion rate of between 4 to 6 km/Ma (Table 1) since
 505 emergence, our calculations suggest that between 25'000 km³ and 115'000 km³ of material may have
 506 bypassed the foreland basin. If this is correct, it suggests that at least half the sediment eroded from the
 507 orogen may not be preserved in the eventual stratigraphic record of the foreland basin. This material is
 508 likely longitudinally transported south out of the basin (Nagel et al., 2013), and into the South China
 509 Sea. Observations in south-central Taiwan already indicate enhanced southward sediment transport
 510 since Late Pliocene marked by increasing amounts of submarine incisions (Fuh et al., 2003; Fuh et al.,
 511 1997). The southward sediment transport is also observed in the migration of sediment depocenters
 512 and facies belts, mainly driven by the large sediment flux from the orogen (Nagel et al., 2013; Simoes
 513 et al., 2007).

514

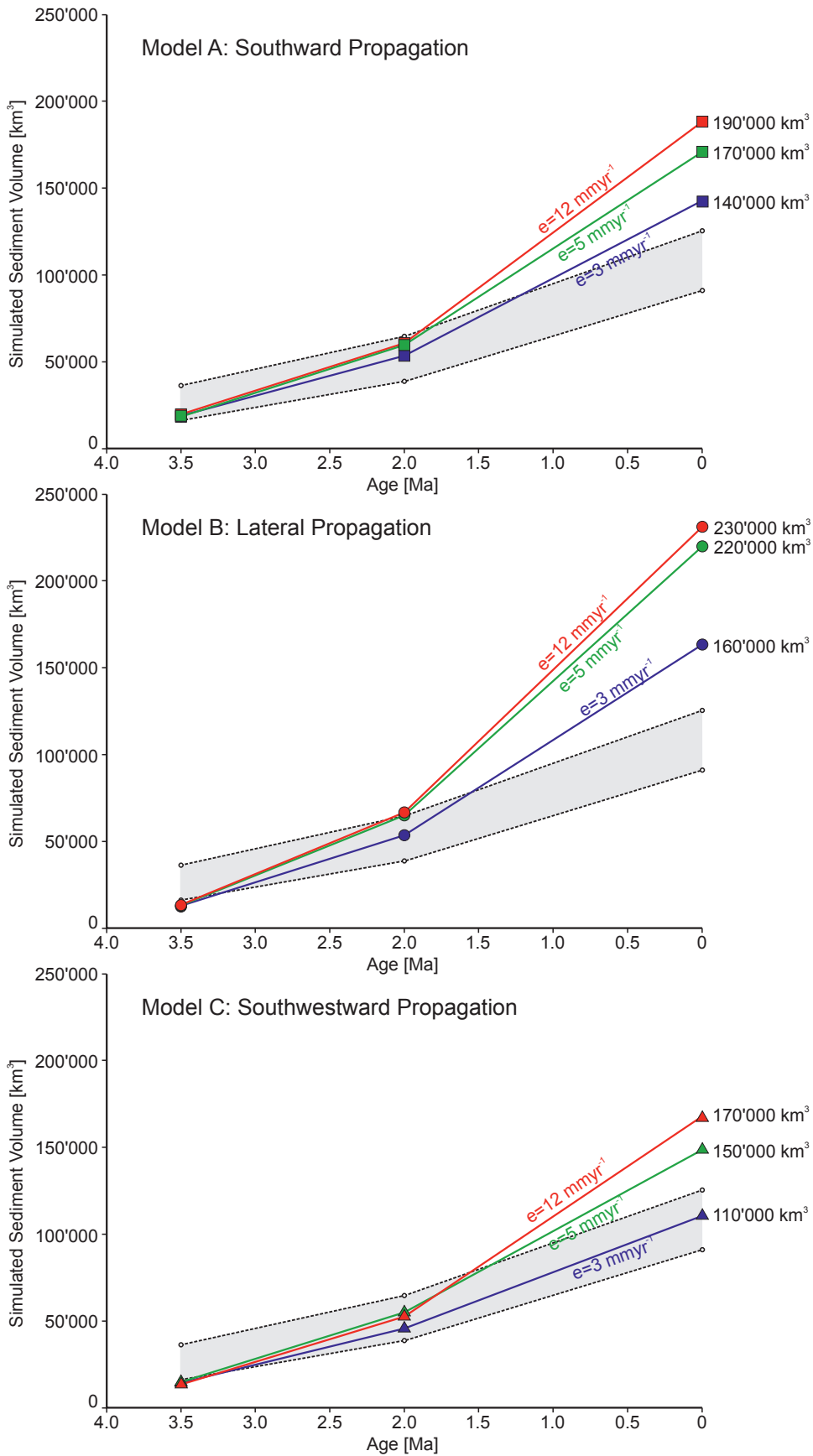
515 4.2. Simulated sediment fluxes

516 An orogen that produces a steady flux of sediments was modeled for each of the three different growth
 517 scenarios in Figure 9 and the volume of material deposited in the basin was calculated for each
 518 scenario (Fig. 13). Steady state is established when the elevation of the mountain top reaches a roughly
 519 constant value in less than 1 Ma. This is achieved by tuning with the diffusion coefficient for
 520 continental sediment transport K , where an increase in K equals an increase in erosion, until a value of
 521 K is found that works for all 3 scenarios. Three different models were run, with a mean uplift rate set
 522 to 3, 5 and 12 mm/yr. Material is allowed to leave the basin to the south by diffusion. The area of the
 523 orogen at each time step is the same for each growth model, thus with identical uplift and erosion
 524 parameters the available material at each interval is assumed to be equal. This allows us to compare all
 525 three models in terms of only the tectonic growth scenario and longitudinal transport efficiency..



526
 527 **Figure 13:** The model setup is shown schematically in Fig. 9. Model A is simulated with a southward propagation rate of 90
 528 km/Ma and a fixed width. In model B the length of the orogen was fixed and only lateral propagation allowed. Model C is a
 529 combined " oblique" collision, or southwestward propagation. In all the three models, the final orogen area and final
 530 erosional fluxes vary only by a minor amount due to different erosional landscape evolution during relief growth. The area
 531 where the simulated foreland basin volume was measured is indicated with a black box.
 532

533 The sediment volume of the foreland basin produced by each of the three models is shown in Figure
 534 14. The three standard models (southward, lateral, or oblique propagation) tend to overestimate the
 535 preserved sediment volume. Southward and oblique propagation achieve a better fit to the observed
 536 sediment thickness than lateral propagation. Moreover lateral propagation did not accurately reproduce
 537 the foreland basin geometries. The best fit (geometry and volume) is achieved with the oblique
 538 collision scenario.



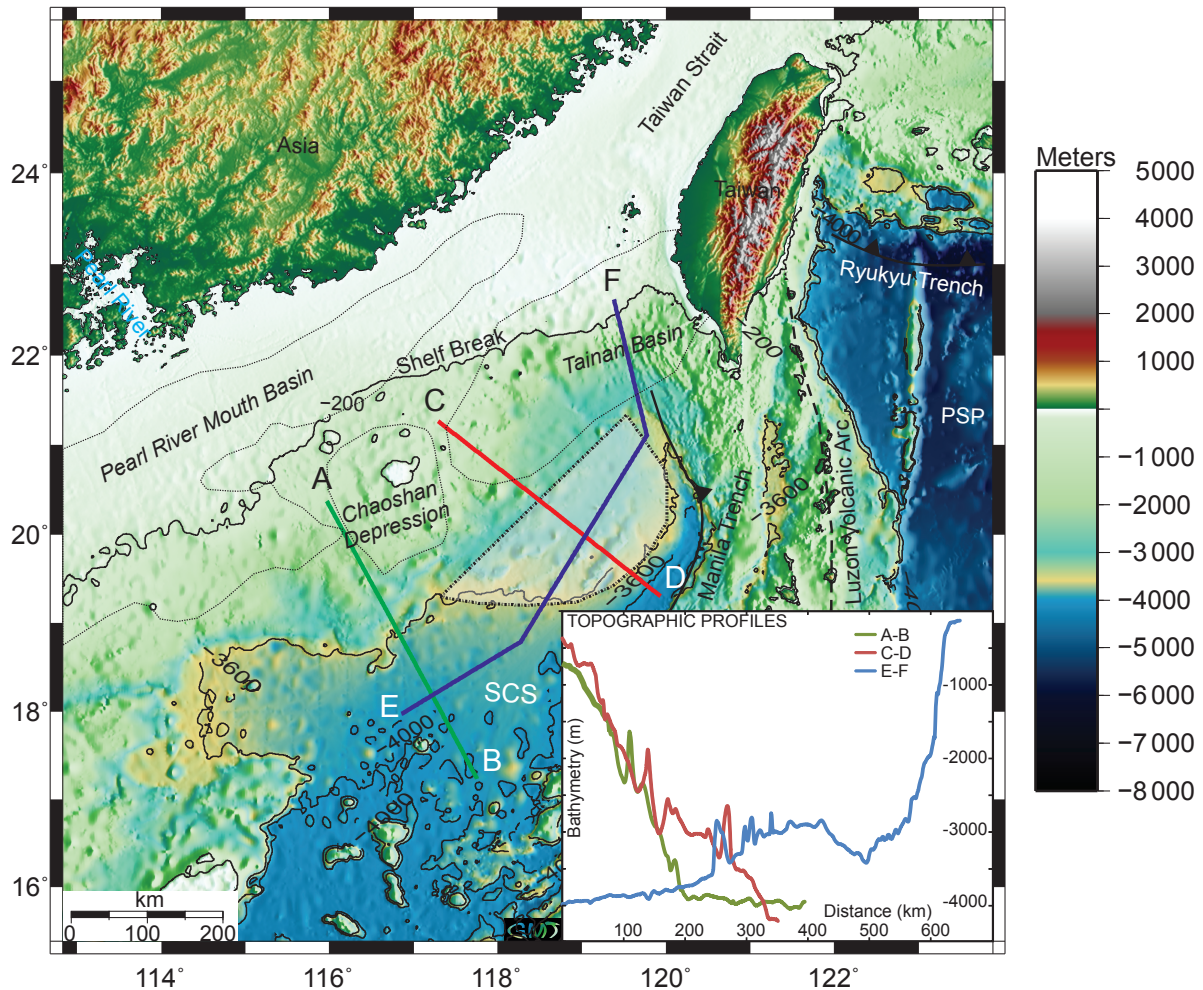
539
540
541
542

Figure 14: Calculated sediment volume in the foreland basin produced with the three standard collision models (Fig. 9). The preserved sediment thickness in the Taiwan foreland basin is between 70-125'000 km³ (shaded area, see also Table 3).

543 The southward propagation models suggest an excess of sediment carried into the basin between 15-
544 $80'000 \text{ km}^3$. This amount is in agreement with the theoretical mass balance calculations (Fig. 12). As
545 observed, even though the orogen reached a steady state size as suggested by (Suppe, 1981), due to
546 longitudinal transport the basin never becomes overfilled.

547 Earlier observations already implied an important longitudinal sediment transport out of the basin and
548 observations from the southwest of Taiwan seem to confirm these predictions (Covey, 1984; Yu and
549 Hong, 2006). Longitudinal sediment transport is common in most foreland basins. A good example is
550 the southern Pyrenees, where longitudinal sediment routing systems dominated a wedge-top depozone,
551 with deep marine sedimentation prevailing (Mutti, 1977, Castelltort et al., 2017). It is important to
552 note in contrast, that an averaged orogen-wide erosion rate of 3 mm/yr produces a sediment volume
553 that is consistent with the preserved sediment volume in the western foreland basin (Fig 14, Model C).
554 This means that, according to our approach, either previous estimates of erosion rate based on
555 thermochronological constraints are too high, or sediment bypass occurred at least for parts of the
556 basin history.

557 Because of the presence of many submarine canyons draining sediment from the Taiwan Strait to the
558 deeper basin in the Manila trench (Damuth, 1979; Yu and Chang, 2002; Yu et al., 2009), a
559 fundamental unknown is whether one can find there the missing sediment volume arising from our
560 calculations. Sparse literature data are available on the nature of the sedimentary basins in the area of
561 the South China Sea close to Taiwan (Lee et al., 1993; Lin et al., 2008; Yu and Huang, 2009), with a
562 main focus on the Pearl River delta and associated submarine fan deposits (Lüdmann et al., 2001; Su
563 et al., 1989; Xiong et al., 2004) (Li et al., 2008). A topographic map of the submarine regions south of
564 Taiwan indicates a peculiarity in the slope of the South China Sea continental margin compared to its
565 continuation further to the south. This suggests an anomalous accumulation of sediment in this area.
566 Topographic profiles across and along the continental margin (Fig. 15, inset) show that the ocean floor
567 remains at a bathymetry of about -4000 m. As a first order approximation we use the isobath -3600 m
568 and a line roughly parallel to the shelf edge to delimit the contour of this promontory of the continental
569 margin and to compute its volume. The volume enclosed by the area drawn on Figure 15 and using -
570 4000 m as a base elevation represents $28'700 \text{ km}^3$ ($15'400 \text{ km}^3$ when -3600 m is used as a base
571 elevation for the calculation).



572
 573 **Figure 15:** Calculated sediment volume in the northern South China Sea based on topographic profiles across and along the
 574 Asian continental margin. The volume stored in the area (dashed line) represents $\sim 30'000 \text{ km}^3$.
 575

576 The volume of this submarine topography is compatible with deposits originated in the Taiwan
 577 orogeny that would have bypassed the Taiwan Strait. The outline of the Tainan basin on the
 578 topographic map of figure 15 and its southwestward orientation visible on the paleogeographic maps
 579 of figure 4 show that the Tainan basin may have constituted a longitudinal through working as a
 580 conduit for material sourced in the Taiwan orogenic wedge. In this case, a non-negligible portion of
 581 the sedimentary record of mountain building may have been preserved outside of the foreland basin
 582 itself. However this hypothesis remains to be tested with future work investigating the
 583 sedimentological nature and stratigraphy of this anomalous promontory and look for potential
 584 sediment depocenters outside of the Taiwan Strait. This finding outlines the potential complexity of
 585 interpreting provenance signals (Romans et al., 2016) in orogen-basin systems with highly dynamic
 586 topographic evolution.

587

588 5. Conclusions

589 The sedimentary system of the Taiwan foreland basin is governed by the oblique collision
 590 between the Luzon volcanic arc and the Asian passive margin. Different geometrical models
 591 of orogen growth and its influence on the basin architecture were tested by means of a
 592 stratigraphic modeling approach. We observe that by looking at the sediment volume in the

593 foreland basin and calculating mass flux sediment budgets, a significant (perhaps more than
594 50%) portion of the sediment eroded from the orogen is not preserved in the stratigraphic
595 record of the immediately adjacent foreland basin. The excess sediment is most likely
596 transported northward into the Okinawa Trough and southward into the South China Sea,
597 where large submarine channel-lobe systems developed. This interpretation is consistent with
598 an increasing amount of submarine incisions since Late Pliocene observed in southwest
599 Taiwan.

600 We propose that this may be one possible explanation as to why despite reaching a steady
601 state, the basin remains underfilled. We tested three different orogenic growth scenarios with
602 longitudinal transport. While predicted preserved sediment thicknesses exceeded observed
603 sediment thickness, longitudinal transport was efficient enough to keep the basin from
604 overfilling in all three scenarios. However, we find that, despite recent suggestions that
605 collision in Taiwan may have been synchronous along its entire length (Castelltort et al.,
606 2011, Lee et al., 2015), an oblique collision fits better the observed basin architecture.

607

608 **Acknowledgements**

609 This work was funded by Swiss National Science Foundation grant #200020-131890 to SC.

610 **References**

- 611 Abbott, L.D., Silver, E.A., Thompson, P.R., Filewicz, M.V., Schneider, C., Abdoerrias, 1994. Stratigraphic
612 constraints on the development and timing of arc-continent collision in northern Papua New Guinea. *J.*
613 *Sediment. Res.* 64, 169-183.
- 614 Allen, P.A., Allen, J.R., 2009. *Basin Analysis: Principles and Applications*. John Wiley & Sons.
- 615 Allen, P.A., Crampton, S.L., Sinclair, H.D., 1991. The inception and early evolution of the North Alpine
616 Foreland Basin, Switzerland. *Basin Res.* 3, 143-163.
- 617 Castelltort, S., Whittaker, A., Vergés, J., 2015. Tectonics, sedimentation and surface processes: from the
618 erosional engine to basin deposition. *Earth Surf. Process. Landforms* 40, 1839–1846. doi:10.1002/esp.3769
- 619 Castelltort, S., Nagel, S., Mouthereau, F., Lin, A.T.-S., Wetzel, A., Kaus, B., D., W.S., Chiang, S.-P., Chiu, W.-
620 Y., 2011. Sedimentology of early Pliocene sandstones in the south-western Taiwan foreland: Implications for
621 basin physiography in the early stages of collision. *J. Asian Earth Sci.* 40, 52-71.
- 622 Castelltort, S., Honegger, L., Adatte, T., Clark, J.D., Puigdefabregas, C., Spangenberg, J.E., Dykstra, M.L.,
623 Fildani, A., 2017. Detecting eustatic and tectonic signals with carbon isotopes in deep-marine strata, Eocene
624 Ainsa Basin, Spanish Pyrenees. *Geology* G39068.1. doi:10.1130/G39068.1
- 625 Chang, S.S.L., Chi, W.-R., 1983. Neogene nannoplankton biostratigraphy in Taiwan and the tectonic
626 implications. *Petroleum Geology of Taiwan* 19, 93-147.
- 627 Chang S. L., J. Yuan, P. T. Hsiao, and W. R. Chi, 1983, The Neogene series, tectonic evolution and petroleum
628 potentialities of southwestern Taiwan, in *Transactions of the Third Circum-Pacific Energy and Mineral*
629 *Resources Conferences*, vol. 3, edited by T. Wilson-Stuart, pp. 577 – 587.
- 630 Chen, W.-S., Ridgway, K.D., Horng, C.-S., Chen, Y.-G., Shea, K.-S., Yeh, M.-G., 2001a. Stratigraphic
631 architecture, magnetostratigraphy and incised-valley systems of the Pliocene-Pleistocene collisional marine
632 foreland basin Taiwan. *Geol. Soc. Am. Bull.* 113, 1249-1271.
- 633 Chen, Z., Li, J., Shen, H., Zhanghua, W., 2001b. Yangtze River of China: historical analysis of discharge
634 variability and sediment flux. *Geomorphology* 41, 77-91.
- 635 Chiang, C.-S., Yu, H.-S., Chou, Y.-W., 2004. Characteristics of the wedge-top depozone of the southern Taiwan
636 foreland basin system. *Basin Res.* 16, 65-78.
- 637 Chiu, H.T., 1975. Miocene stratigraphy and its relation to the palaeogene rocks in west-central Taiwan.
638 *Petroleum Geology of Taiwan* 12, 51-80.

- 639 Chou, J.-T., 1973. Sedimentology and paleogeography of the upper Cenozoic system of Western Taiwan.
640 Proceedings of the Geological Society of China 16, 111-143.
- 641 Covey, M., 1984. Sedimentary and tectonic evolution of the western Taiwan Foredeep. Unpublished Ph.D.
642 thesis.
- 643 Covey, M., 1986. The Evolution of Foreland Basins to Steady State: Evidence from the Western Taiwan
644 Foreland Basin, Foreland Basins. Blackwell Publishing Ltd., pp. 77-90.
- 645 Dadson, S., Hovius, N., Pegg, S., Dade, W.B., Horng, M.J., Chen, H., 2005. Hyperpycnal river flows from an
646 active mountain belt. *J. Geophys. Res.* 110, F04016.
- 647 Dadson, S.J., Hovius, N., Chen, H., Dade, W.B., Hsieh, M.L., Willett, S.D., Hu, J.C., Horng, M.J., Chen, M.C.,
648 Stark, C.P., Lague, D., Lin, J.C., 2003. Links between erosion, runoff variability and seismicity in the Taiwan
649 Orogen. *Nature (London)* 426, 648-651.
- 650 Damuth, J.E., 1979. Migrating sediment waves created by turbidity currents in the northern South China Basin.
651 *Geology* 7, 520-523.
- 652 Dorsey, R.J., Buchovecky, E.J., Lundberg, N., 1988. Clay mineralogy of Pliocene-Pleistocene mudstones,
653 eastern Taiwan: combined effects of burial diagenesis and provenance unroofing. *Geology* 16, 944-947.
- 654 Dorsey, R.J., Lundberg, N., 1988. Lithofacies analysis and basin reconstruction of the Plio-Pleistocene
655 collisional basin, Coastal Range of Eastern Taiwan. *Acta Geol. Taiwan.* 26, 57-132.
- 656 Flemings, P.B., Jordan, T.E., 1989. A Synthetic Stratigraphic Model of Foreland Basin Development. *J.*
657 *Geophys. Res.* 94, 3851-3866.
- 658 Fuh, S.-C., Liang, S.-C., Wu, M.-S., 2003. Spatial and temporal evolution of the Plio-Pleistocene submarine
659 canyons between Potzu and Tainan, Taiwan. *Petroleum Geology of Taiwan* 36, 1-18.
- 660 Fuh, S.-C., Liu, C.-S., Wu, M.-S., 1997. Migration of canyon systems from Pliocene to Pleistocene in area
661 between Hsuning structure and Kaoping slope and its application for hydrocarbon exploration. *Petroleum*
662 *Geology of Taiwan* 31.
- 663 Fuller, C., Willett, S.D., Hovius, N., Slingerland, R., 2003. Erosion Rates for Taiwan Mountain Basins: New
664 Determinations from Suspended Sediment Records and a Stochastic Model of Their Temporal Variation. *The*
665 *Journal of Geology* 111, 71-87.
- 666 Fuller, C.W., Willett, S.D., Fisher, D., Lu, C.Y., 2006. A thermomechanical wedge model of Taiwan constrained
667 by fission-track thermochronometry. *Tectonophysics* 425, 1-24.
- 668 Garzanti, E., Vezzoli, G., Andò, S., Paparella, P., Clift, P.D., 2005. Petrology of Indus River sands: a key to
669 interpret erosion history of the Western Himalayan Syntaxis. *Earth Planet. Sci. Lett.* 229, 287-302.
- 670 Garzanti, E., Vezzoli, G., Lombardo, B., Andò, S., Mauri, E., Monguzzi, S., Russo, M., 2004. Collision-orogen
671 provenance (Western Alps): detrital signatures and unroofing trends. *The Journal of Geology* 112, 145-164.
- 672 Granjeon, D., 1997. Modélisation stratigraphique déterministe: conception et applications d'un modèle diffusif
673 3D multilithologique, Géosciences. Université de Rennes, Rennes, 200 p.
- 674 Granjeon, D., Joseph, P., 1999. Concepts and applications of a 3-D multiple lithology, diffusive model in
675 stratigraphic modeling, in: Harbaugh, J.W., Watney, W.L., Rankey, E.C., Slingerland, R., Goldstein, R.H.,
676 Franseen, E.K. (Eds.), *Numerical Experiments in Stratigraphy*. SEPM (Society for Sedimentary Geology), pp.
677 197-210.
- 678 Hall, R., 1996. Reconstructing Cenozoic SE Asia. Geological Society, London, Special Publications 106, 153-
679 184.
- 680 Hicks, D.M., Gomez, B., Trustrum, N.A., 2000. Erosion thresholds and suspended sediment yields, Waipaoa
681 River Basin, New Zealand. *Water Resour. Res.* 36, 1129-1142.
- 682 Ho, C.S., 1988. An introduction to the geology of Taiwan: explanatory text of the geologic map of Taiwan, 2nd
683 ed. Central Geological Survey, The Ministry of Economic Affairs, R.O.C. Taiwan.
- 684 Horng, C.-S., Huh, C.-A., 2011. Magnetic properties as tracers for source-to-sink dispersal of sediments: A case
685 study in the Taiwan Strait. *Earth Planet. Sci. Lett.* 309, 141-152.
- 686 Horng, C.-S., Huh, C.-A., Chen, K.-H., Lin, C.-H., Shea, K.-S., Hsiung, K.-H., 2012. Pyrrhotite as a tracer for
687 denudation of the Taiwan orogen. *Geochem. Geophys. Geosyst.* 13, Q08Z47.
- 688 Horng, C.-S., Shea, K.-S., 1994. Study of nannofossil biostratigraphy in the Eastern part of the Erhjen-Chi
689 section, Southwestern Taiwan. Special Publication of the Central Geological Survey 8, 181-204.

- 690 Hsu, W.-H., Byrne, T.B., Ouimet, W., Lee, Y.-H., Chen, Y.-G., Soest, M.V., Hodges, K., 2016. Pleistocene
691 onset of rapid, punctuated exhumation in the eastern Central Range of the Taiwan orogenic belt. *geology* 44,
692 719–722. doi:10.1130/G37914.1
- 693 Hu, J., Kawamura, H., Li, C., Hong, H., Jiang, Y., 2010. Review on current and seawater volume transport
694 through the Taiwan Strait. *J. Oceanogr.* 66, 591-610.
- 695 Huang, C.-Y., Yuan, P.B., Tsao, S.-J., 2006. Temporal and spatial records of active arc-continent collision in
696 Taiwan: A synthesis. *GSA Bulletin* 118, 274-288.
- 697 Huang, T.-C., 1976. Neogene calcareous nannoplankton biostratigraphy viewed from the Chuhuangkeng section,
698 Northwestern Taiwan. *Proceedings of the Geological Society of China* 19, 7-24.
- 699 Huang, T., 1977. Late neogene planktonic foraminiferal biostratigraphy of the Tainan Foothills region, Tainan,
700 Taiwan. *Petroleum Geology of Taiwan* 14, 121-145.
- 701 Huang, T., Huang, T.-C., 1984. Neogene biostratigraphy of Taiwan, in: Ikebe, N., Tsuchi, R. (Eds.), *Pacific*
702 *Neogen Datum Planes: contributions to biostratigraphy and chronology*. University of Tokyo Press.
- 703 Huh, C.-A., Chen, W., Hsu, F.-H., Su, C.-C., Chiu, J.-K., Lin, S., Liu, C.-S., Huang, B.-J., 2011. Modern (<100
704 years) sedimentation in the Taiwan Strait: Rates and source-to-sink pathways elucidated from radionuclides and
705 particle size distribution. *Cont. Shelf Res.* 31, 47-63.
- 706 Jan, S., Wang, J., Chern, C.-S., Chao, S.-Y., 2002. Seasonal variation of the circulation in the Taiwan Strait.
707 *Journal of Marine Systems* 35, 249-268.
- 708 Kao, H., Huang, G.-C., Liu, C.-S., 2000. Transition from oblique subduction to collision in the northern Luzon
709 arc-Taiwan region: Constraints from bathymetry and seismic observations. *J. Geophys. Res.* 105, 3059-3079.
- 710 Kao, S.-J., Jan, S., Hsu, S.-C., Lee, T.-Y., Dai, M., 2008. Sediment budget in the Taiwan Strait with high fluvial
711 sediment inputs from mountainous rivers: new observations and synthesis. *Terr. Atmos. Ocean Sci.* 19, 525-546.
- 712 Kao, S.J., Milliman, J.D., 2008. Water and Sediment Discharge from Small Mountainous Rivers, Taiwan: The
713 Roles of Lithology, Episodic Events, and Human Activities. *The Journal of Geology* 116, 431-448.
- 714 Kineke, G.C., Woolfe, K.J., Kuehl, S.A., Milliman, J.D., Dellapenna, T.M., Purdon, R.G., 2000. Sediment export
715 from the Sepik River, Papua New Guinea: evidence for a divergent sediment plume. *Cont. Shelf Res.* 20, 2239-
716 2266.
- 717 Kniskern, T.A., Kuehl, S.A., Harris, C.K., Carter, L., 2010. Sediment accumulation patterns and fine-scale strata
718 formation on the Waiapu River shelf, New Zealand. *Mar. Geol.* 270, 188-201.
- 719 Kuehl, S.A., Brunskill, G.J., Burns, K., Fugate, D., Kniskern, T., Meneghini, L., 2004. Nature of sediment
720 dispersal off the Sepik River, Papua New Guinea: preliminary sediment budget and implications for margin
721 processes. *Cont. Shelf Res.* 24, 2417-2429.
- 722 Lee, T.-Y., Lawver, L.A., 1995. Cenozoic plate reconstruction of Southeast Asia. *Tectonophysics* 251, 85-138.
- 723 Lee, T.-Y., Tang, C.H., Ting, J.-S., Hsu, Y.-Y., 1993. Sequence stratigraphy of the Tainan Basin, offshore
724 Southwestern Taiwan. *Petroleum Geology of Taiwan* 28, 119-158.
- 725 Lee, Y.-H., Chen, C.-C., Liu, T.-K., Ho, H.-C., Lu, H.-Y., Lo, W., 2006. Mountain building mechanisms in the
726 Southern Central Range of the Taiwan Orogenic Belt - From accretionary wedge deformation to arc-continent
727 collision. *Earth Planet. Sci. Lett.* 252, 413-422.
- 728 Lee, Y.H., Byrne, T., Wang, W.H., Lo, W., Rau, R.J., Lu, H.Y., 2015. Simultaneous mountain building in the
729 Taiwan orogenic belt. *geology* 43, 451–454. doi:10.1130/G36373.1
- 730 Li, C.-F., Zhou, Z., Hao, H., Chen, H., Wang, J., Chen, B., Wu, J., 2008. Late Mesozoic tectonic structure and
731 evolution along the present-day northeastern South China Sea continental margin. *J. Asian Earth Sci.* 31, 546-
732 561.
- 733 Liao, H.-R., Yu, H.-S., Su, C.-C., 2008. Morphology and sedimentation of sand bodies in the tidal shelf sea of
734 eastern Taiwan Strait. *Mar. Geol.* 248, 161-178.
- 735 Lihou, J.C., Allen, P.A., 1996. Importance of inherited rift margin structures in the early North Alpine Foreland
736 Basin, Switzerland. *Basin Res.* 8, 425-442.
- 737 Lin, A.T., Liu, C.-S., Lin, C.-C., Schnurle, P., Chen, G.-Y., Liao, W.-Z., Teng, L.S., Chuang, H.-J., Wu, M.-S.,
738 2008. Tectonic features associated with the overriding of an accretionary wedge on top of a rifted continental
739 margin: An example from Taiwan. *Mar. Geol.* 255, 186-203.
- 740 Lin, A.T., Watts, A.B., 2002. Origin of the West Taiwan basin by orogenic loading and flexure of a rifted
741 continental margin. *J. Geophys. Res.* 107, 2185.

- 742 Lin, A.T., Watts, A.B., Hesselbo, S.P., 2003. Cenozoic stratigraphy and subsidence history of the South China
743 Sea margin in the Taiwan region. *Basin Res.* 15, 453-478.
- 744 Liu, J.P., Liu, C.S., Xu, K.H., Milliman, J.D., Chiu, J.K., Kao, S.J., Lin, S.W., 2008. Flux and fate of small
745 mountainous rivers derived sediments into the Taiwan Strait. *Mar. Geol.* 256, 65-76.
- 746 Liu, J.P., Xu, K.H., Li, A.C., Milliman, J.D., Velozzi, D.M., Xiao, S.B., Yang, Z.S., 2007. Flux and fate of
747 Yangtze river sediment delivered to the East China Sea. *Geomorphology* 85, 208-224.
- 748 Liu, T.-K., Hsieh, S., Chen, Y.-G., Chen, W.-S., 2001. Thermo-kinematic evolution of the Taiwan oblique-
749 collision mountain belt as revealed by zircon fission track dating. *Earth Planet. Sci. Lett.* 186, 45-56.
- 750 Liu, T.K., Chen, Y.G., Chen, W.S., Jiang, S.H., 2000. Rates of cooling and denudation of the Early Penglai
751 Orogeny, Taiwan, as assessed by fission-track constraints. *Tectonophysics* 320, 69-82.
- 752 Liu, Z., Colin, C., Li, X., Zhao, Y., Tuo, S., Chen, Z., Siringan, F.P., Liu, J.T., Huang, C.-Y., You, C.-F., Huang,
753 K.-F., 2010. Clay mineral distribution in surface sediments of the northeastern South China Sea and surrounding
754 fluvial drainage basins: Source and transport. *Mar. Geol.* 277, 48-60.
- 755 Liu, Z., Trentesaux, A., Clemens, S.C., Colin, C., Wang, P., Huang, B., Boulay, S., 2003. Clay mineral
756 assemblages in the northern South China Sea: implications for East Asian monsoon evolution over the past 2
757 million years. *Mar. Geol.* 201, 133-146.
- 758 Lock, J., 2007. *Interpreting Low-temperature Thermochronometric Data in Fold-and-thrust Belts: An Example*
759 *from the Western Foothills, Taiwan.* University of Washington.
- 760 Lu, C.-Y., Hsü, K.J., 1992. Tectonic evolution of the Taiwan mountain belt. *Petroleum Geology of Taiwan* 27,
761 21-46.
- 762 Lüdman, T., Kin Wong, H., Wang, P., 2001. Plio-Quaternary sedimentation processes and neotectonics of the
763 northern continental margin of the South China Sea. *Mar. Geol.* 172, 331-358.
- 764 Lundberg, N., Dorsey, R.J., 1990. Rapid Quaternary emergence, uplift, and denudation of the Coastal Range,
765 Eastern Taiwan. *Geology* 18, 638-641.
- 766 Meng, C.-Y., 1967. The structural development of the southern half of western Taiwan. *Proceedings of the*
767 *Geological Society of China* 10, 77-82.
- 768 Métivier, F., Gaudemer, Y., Tapponnier, P., Klein, M., 1999. Mass accumulation rates in Asia during the
769 Cenozoic. *Geophys. J. Int.* 137, 280-318.
- 770 Miller, K.G., Mountain, G.S., Wright, J.D., Browning, J.V., 2011. A 180-Million-Year Record of Sea Level and
771 Ice Volume Variations from Continental Margin and Deep-Sea Isotopic Records. *Oceanography* 24, 40-53.
- 772 Milliman, J.D., Kao, S.-J., 2005. Hyperpycnal discharge of fluvial sediment to the ocean: impact of super-
773 Typhoon Herb (1996) on Taiwanese rivers. *The Journal of Geology* 113, 503-516.
- 774 Milliman, J.D., Lin, S.W., Kao, S.J., Liu, J.P., Liu, C.S., Chiu, J.K., Lin, Y.C., 2007. Short-term changes in
775 seafloor character due to flood-derived hyperpycnal discharge: Typhoon Mindulle, Taiwan, July 2004. *Geology*
776 35, 779-782.
- 777 Milliman, J.D., Syvitski, J.P.M., 1992. Geomorphic/Tectonic Control of Sediment Discharge to the Ocean: The
778 Importance of Small Mountainous Rivers. *J. Geol.* 100, 525-544.
- 779 Mouthereau, F., Lacombe, O., 2006. Inversion of the Paleogene Chinese continental margin and thick-skinned
780 deformation in the Western Foreland of Taiwan. *J. Struct. Geol.* 28, 1977-1993.
- 781 Mouthereau, F., Lacombe, O., Deffontaines, B., Angelier, J., Brusset, S., 2001. Deformation history of the
782 southwestern Taiwan foreland thrust belt: insights from tectono-sedimentary analyses and balanced cross-
783 sections. *Tectonophysics* 333, 293-322.
- 784 Mutti, E., 1977. Distinctive thin-bedded turbidite facies and related depositional environments in the Eocene
785 Hecho Group (South-central Pyrenees, Spain). *Sedimentology* 24, 107-131.
- 786 Nagel, S., Castelltort, S., D., W.S., Mouthereau, F., Lin, A.T., (in preparation). Tectono-sedimentary evolution of
787 a doubly vergent orogen; an example from the Western foredeep, Taiwan. (in preparation).
- 788 Nagel, S., Castelltort, S., Wetzels, A., Willett, S.D., Mouthereau, F., Lin, A.T., 2013. Sedimentology and foreland
789 basin paleogeography during Taiwan arc continent collision. *J. Asian Earth Sci.* (10.1016/j.jseaes.2012.09.001).
- 790 Naylor, M., Sinclair, H.D., 2008. Pro- vs. retro-foreland basins. *Basin Res.* 20, 285-303.
- 791 Olariu, C., Steel, R.J., 2009. Influence of point-source sediment-supply on modern shelf-slope morphology:
792 implications for interpretation of ancient shelf margins. *Basin Res.* 21, 484-501.

- 793 Pan, T.-S., 2011. A study on sedimentary environments of Nanchuang Formation to Yangmei Formation along
794 the Dahan River section, northwestern Taiwan, Department of Earth Sciences. National Central University,
795 Jhongli.
- 796 Pelletier, B., Stephan, J.F., 1986. Middle Miocene obduction and late Miocene beginning of collision registered
797 in the Hengchun Peninsula: geodynamic implications for the evolution of Taiwan. *Tectonophysics* 125, 133-160.
- 798 Puigdefàbregas, C., Muñoz, J.A., Vergés, J., 1992. Thrusting and foreland basin evolution in the southern
799 Pyrenees, in: McClay, K. (Ed.), *Thrust tectonics*. Chapman & Hall, London, pp. 247-254.
- 800 Resentini, A., L. Goren, S. Castellort, and E. Garzanti (2017), Partitioning sediment flux by provenance and
801 tracing erosion patterns in Taiwan, *J. Geophys. Res. Earth Surf.*, 122, doi:10.1002/2016JF004026.
- 802 Romans, B.W., Castellort, S., Covault, J.A., Fildani, A., Walsh, J.P., 2016. Environmental signal propagation in
803 sedimentary systems across timescales. *Earth Science Reviews* 153, 7–29. doi:10.1016/j.earscirev.2015.07.012
- 804 Seno, T., Kawanishi, Y., 2009. Reappraisal of the Arc-Arc Collision in Taiwan. *Terr. Atmos. Ocean Sci.* 20,
805 573-585.
- 806 Seno, T., Stein, S., Grip, A.E., 1993. A model for the motion of the Philippine Sea plate consistent with
807 NUVEL-1 and geologic data. *J. Geophys. Res.* 98 (B10), 941–948.
- 808 Shaw, C.-L., 1996. Stratigraphic correlation and isopach maps of the Western Taiwan Basin. *Terr. Atmos. Ocean*
809 *Sci.* 7, 333-360.
- 810 Siame, L.L., Angelier, J., Chen, R.F., Godard, V., Derrieux, F., Bourlès, D.L., Braucher, R., Chang, K.J., Chu,
811 H.T., Lee, J.C., 2011. Erosion rates in an active orogen (NE-Taiwan): A confrontation of cosmogenic
812 measurements with river suspended loads. *Quat. Geochronol.* 6, 246-260.
- 813 Sibuet, J.-C., Hsu, S.-K., 1997. Geodynamics of the Taiwan arc-arc collision. *Tectonophysics* 274, 221-251.
- 814 Sibuet, J.-C., Hsu, S.-K., 2004. How was Taiwan created? *Tectonophysics* 379, 159-181.
- 815 Sibuet, J.-C., Hsu, S.-K., Shyu, C.-T., Liu, C.S., 1995. Structural and kinematic evolutions of the Okinawa
816 trough backarc basin, in: Taylor, B. (Ed.), *Backarc Basins: Tectonics and Magmatism*. Plenum Press.
- 817 Silver, E.A., Abbott, L.D., Kirchoff-Stein, K.S., Reed, D.L., Bernstein-Taylor, B., Hilyard, D., 1991. Collision
818 propagation in Papua New Guinea and the Solomon Sea. *Tectonics* 10, 863-874.
- 819 Simoes, M., Avouac, J.P., Beyssac, O., Goffé, B., Farley, K.A., Chen, Y.-G., 2007. Mountain building in
820 Taiwan: A thermokinematic model. *J. Geophys. Res.* 112, B11405.
- 821 Simoes, M., Avouac, P., 2006. Investigating the kinematics of mountain building in Taiwan from the
822 spatiotemporal evolution of the foreland basin and western foothills. *J. Geophys. Res.* 11.
- 823 Sinclair, H.D., Coakley, B.J., Allen, P.A., Watts, A.B., 1991. Simulation of foreland basin stratigraphy using a
824 diffusion-model of mountain belt uplift and erosion - an example from the central Alps, Switzerland. *Tectonics*
825 10, 599-620.
- 826 Sinclair, H.D., Naylor, M., 2012. Foreland basin subsidence driven by topographic growth versus plate
827 subduction. *Geol. Soc. Am. Bull.* 124, 368-379.
- 828 Sømme, T.O., Helland-Hansen, W., Martinsen, O.J., Thurmond, J.B., 2009. Relationships between
829 morphological and sedimentological parameters in source-to-sink systems: a basis for predicting semi-
830 quantitative characteristics in subsurface systems. *Basin Res.* 21, 361-387.
- 831 Stolar, D.B., Willett, S.D., Montgomery, D.R., 2007. Characterization of topographic steady state in Taiwan.
832 *Earth Planet. Sci. Lett.* 261, 421-431.
- 833 Su, D., White, N., McKenzie, D.A.N., 1989. Extension and subsidence of the Pearl River Mouth Basin, northern
834 South China Sea. *Basin Res.* 2, 205-222.
- 835 Suppe, J., 1981. Mechanics of mountain-building and metamorphism in Taiwan. *Memoir of the Geological*
836 *Society of China* 4, 67-89.
- 837 Suppe, J., 1984. Kinematics of arc-continent collision, flipping of subduction, and back-arc spreading near
838 Taiwan. *Memoir of the geological society of China* 6, 21-33.
- 839 Suppe, J., 1988. Tectonics of arc-continent collision on both sides of the south China sea: Taiwan and Mindoro.
840 *Acta Geol. Taiwan.* 26, 1-18.
- 841 Teng, L.S., 1990. Geotectonic evolution of late Cenozoic arc-continent collision in Taiwan. *Tectonophysics* 183,
842 57-76.
- 843 Tensi, J., Mouthereau, F., Lacombe, O., 2006. Lithospheric bulge in the West Taiwan Basin. *Basin Res.* 18, 277-
844 299.

- 845 Ting, H.-H., Huang, C.-Y., Wu, L.-C., 1991. Paleoenvironments of the late neogene sequences along the
846 Nantzuhsien river, Southern Taiwan. *Petroleum Geology of Taiwan* 26, 121-149.
- 847 Tropeano, M., Sabato, L., Pieri, P., 2002. Filling and cannibalization of a foredeep: the Bradanic Trough,
848 Southern Italy. Geological Society, London, Special Publications 191, 55-79.
- 849 Vergés, J., Burbank, D.W., 1996. Eocene-Oligocene thrusting and basin configuration in the eastern and central
850 Pyrenees (Spain), in: Friend, Dabrio (Eds.), *Tertiary Basins of Spain*, Cambridge University Press ed, pp. 120-
851 133.
- 852 Wan, S., Li, A., Clift, P.D., Jiang, H., 2006. Development of the East Asian summer monsoon: Evidence from
853 the sediment record in the South China Sea since 8.5 Ma. *Palaeogeography, Palaeoclimatology, Palaeoecology*
854 241, 139-159.
- 855 Wang, H., Yang, Z., Saito, Y., Liu, J.P., Sun, X., Wang, Y., 2007. Stepwise decreases of the Huanghe (Yellow
856 River) sediment load (1950–2005): Impacts of climate change and human activities. *Global Planet. Change* 57,
857 331-354.
- 858 Wang, S., Chen, Z., Smith, D.G., 2005. Anastomosing river system along the subsiding middle Yangtze River
859 basin, southern China. *Catena* 60, 147-163.
- 860 Watts, A.B., Ryan, W.B.F., 1976. Flexure of the lithosphere and continental margin basins. *Tectonophysics* 36,
861 25-44.
- 862 White, N.M., Pringle, M., Garzanti, E., Bickle, M., Najman, Y., Chapman, H., Friend, P., 2002. Constraints on
863 the exhumation and erosion of the high Himalayan slab, NW India, from foreland basin deposits. *Earth Planet.*
864 *Sci. Lett.* 195, 29-44.
- 865 Willett, S.D., Brandon, M.T., 2002. On steady state in mountains belts. *Geology* 30, 175-178.
- 866 Willett, S.D., Fisher, D., Fuller, C., En-Chao, Y., Chia-Yu, L., 2003. Erosion rates and orogenic-wedge
867 kinematics in Taiwan inferred from fission-track thermochronometry. *Geology* 31, 945-948.
- 868 Wolanski, E., King, B., Galloway, D., 1995. Dynamics of the turbidity maximum in the Fly River estuary, Papua
869 New Guinea. *Estuar. Coast. Shelf Sci.* 40, 321-337.
- 870 Wu, W.-N., Hsu, S.-K., Lo, C.-L., Chen, H.-W., Ma, K.-F., 2009. Plate convergence at the westernmost
871 Philippine Sea Plate. *Tectonophysics* 466, 162-169.
- 872 Wu, Y.-M., Chang, C.-H., Zhao, L., Shyu, J.B.H., Chen, Y.-G., Sieh, K., Avouac, J.-P., 2007. Seismic
873 tomography of Taiwan: Improved constraints from a dense network of strong motion stations. *J. Geophys. Res.*
874 112, B08312.
- 875 Xiong, P., Shaokun, Y., Ming, Z.H.U., Jinsong, L.I., 2004. Deep-water Fan Systems and Petroleum Resources
876 on the Northern Slope of the South China Sea. *Acta Geologica Sinica - English Edition* 78, 626-631.
- 877 Xu, K., Milliman, J.D., Li, A., Paul Liu, J., Kao, S.-J., Wan, S., 2009. Yangtze- and Taiwan-derived sediments
878 on the inner shelf of East China Sea. *Cont. Shelf Res.* 29, 2240-2256.
- 879 Yang, B.C., Chun, S.S., 2001. A seasonal model of surface sedimentation on the Baeksu open-coast intertidal
880 flat, southwestern coast of Korea. *Geosci. J.* 5, 251-262.
- 881 Yang, T.F., Tien, J.-I., Chen, C.-H., Lee, T., Punongbayan, R.S., 1995. Fission-track dating of volcanics in the
882 northern part of the Taiwan-Luzon Arc: eruption ages and evidence for crustal contamination. *J. Southeast.*
883 *Asian Earth Sci.* 11, 81-93.
- 884 Yeh, M.-G., Chang, Y.-L., 1991. The ichnofacies study of the Ailiaochiao formation, the Changchihkung
885 formation, Chiahsien-Meinung area, Kaohsiung. *Petroleum Geology of Taiwan* 26, 151-181.
- 886 Yeh, M.-G., Yang, C.-Y., 1994. Depositional environments of the upper Miocene to Pleistocene series in the
887 Chungpu area, Chiayi, Taiwan. *Petroleum Geology of Taiwan* 29, 193-224.
- 888 Yu, H.-S., Chang, J.-F., 2002. The Penghu Submarine Canyon off Southwestern Taiwan: Morphology and
889 Origin. *Terr. Atmos. Ocean Sci.* 13, 547-562.
- 890 Yu, H.-S., Chiang, C.-S., Shen, S.-M., 2009. Tectonically active sediment dispersal system in SW Taiwan
891 margin with emphasis on the Gaoping (Kaoping) Submarine Canyon. *Journal of Marine Systems* 76, 369-382.
- 892 Yu, H.-S., Chou, Y.-W., 2001. Characteristics and development of the flexural forebulge and basal unconformity
893 of western Taiwan foreland Basin. *Tectonophysics* 333, 277-291.
- 894 Yu, H.-S., Hong, E., 2006. Shifting submarine canyons and development of a foreland basin in SW Taiwan:
895 controls of foreland sedimentation and longitudinal sediment transport. *J. Asian Earth Sci.* 27, 922-932.
- 896 Yu, H.-S., Huang, C.-S., Ku, J.-W., 1991. Morphology and possible origin of the Kaoping submarine canyon
897 head off SW Taiwan. *Acta Geol. Taiwan.* 27, 40-50.

- 898 Yu, H.-S., Huang, Z.-Y., 2006. Intraslope Basin, Seismic Facies and Sedimentary Processes in the Kaoping
899 Slope, Offshore Southwestern Taiwan. *Terr. Atmos. Ocean Sci.* 17, 659-677.
- 900 Yu, H.-S., Huang, Z.-Y., 2009. Morphotectonics and sedimentation in convergent margin basins: An example
901 from juxtaposed marginal sea basin and foreland basin, Northern South China Sea. *Tectonophysics* 466, 241-
902 254.
- 903 Yu, N.-T., Teng, L.S., Chen, W.-S., Yen, I.-C., 2008. Facies characteristics of the upper-Neogene
904 Nantzuhsienchi Section, Kaohsiung, SW Taiwan. *Petroleum Geology of Taiwan* 38, 30-56.
- 905 Yu, S.B., Chen, H.Y., Kuo, L.C., 1997. Velocity of GPS stations in the Taiwan area. *Tectonophysics* 274, 41-59.
- 906 Zhang, S., Lu, X.X., Higgitt, D.L., Chen, C.-T.A., Han, J., Sun, H., 2008. Recent changes of water discharge and
907 sediment load in the Zhujiang (Pearl River) Basin, China. *Global Planet. Change* 60, 365-380.
- 908 Zheng, H., Powell, C.M., Rea, D.K., Wang, J., Wang, P., 2004. Late Miocene and mid-Pliocene enhancement of
909 the East Asian monsoon as viewed from the land and sea. *Global Planet. Change* 41, 147-155.